CHAPTER 1

Bridging Between Experiments and Equations: A Tutorial on Modeling Excitability

David P. McCobb[1] *and Mary Lou Zeeman*[2]

[1]Department of Neurobiology and Behavior, Cornell University, Ithaca, NY, USA
[2]Department of Mathematics, Bowdoin College, Brunswick, ME, USA

The goal of this chapter is to empower collaboration across the disciplines. It is aimed at mathematical scientists who want to better understand neural excitability and experimentalists who want to better understand mathematical modeling and analysis. None of us need to be expert in both disciplines, but each side needs to learn the other's language before our conversations can spark the exciting new collaborations that enrich both disciplines. Learning is an active process:

> *Tell me and I will forget; show me and I may remember; involve me and I will understand.*
>
> –Proverb

We have, therefore, written this chapter to be highly interactive. It is based on the classic model of excitability developed by Morris and Lecar (1981), and built around exercises that introduce the freely available dynamical systems software, XPP (Ermentrout, 2012), to explore and illustrate the modeling concepts. An online graphing calculator, such as Desmos (www.desmos.com), is also used occasionally. The modeling and dynamical systems techniques we develop are extremely versatile, with broad applicability throughout the sciences and social sciences. In the chapters of this volume, they are applied to systems at scales ranging from individual cells to entire neuroendocrine axes. We recommend that you work on the exercises as you read, with plenty of time, and tea and chocolate in hand. It is a great way to learn.

Outline. In Section 1.1, we introduce excitability, encompassing the diversity of action potential waveforms and patterns, recurrent firing, and bursting. We also describe the voltage clamp, the essential tool for dissection of excitability used by Hodgkin and Huxley (1952)

Computational Neuroendocrinology, First Edition. Edited by Duncan J. MacGregor and Gareth Leng.

Companion Website: www.wiley.com/go/Leng/Computational

in their foundational work. In Section 1.2, we introduce the classic, two-dimensional Morris–Lecar model, developed originally from barnacle muscle data to expose the minimal mathematical essence of excitability (Morris and Lecar, 1981). In Sections 1.3 and 1.4, we introduce the software package XPP (see Section 1.3 and Ermentrout (2012)) for download instructions), and use it to explore the model behavior, thereby introducing the language and graphics of dynamical systems and phase-plane analysis. This provides a platform for extending the model and including data from naturally occurring ion channels to dissect the excitability of diverse and more complex cells.

In Sections 1.5–1.10, we follow the seminal paper by Rinzel and Ermentrout (1989) to explore the surprising richness of behavior the Morris–Lecar model can exhibit in response to sustained current injection at various levels. We use three different parameter sets, differing only in the voltage dependence and kinetics of potassium channel gating. For each parameter set, we simulate a current clamp experiment in which sustained current is applied to a cell at rest. In all the three cases, sufficiently high levels of applied current induce tonic spiking, but the onset of spiking occurs through different mechanisms with different properties. With the first parameter set ("Hopf" in Table 1.1), tonic spiking is restricted to a narrow frequency range, as in Hodgkin's Class II, typically resonator, neurons (Hodgkin, 1948). The second parameter set ("SNIC" in Table 1.1) exhibits tonic spiking with arbitrarily low frequency, depending on the applied current, as in Hodgkin's Class I, typically integrator, neurons. The final parameter set ("Homoclinic" in Table 1.1) generates tonic spiking with a high baseline between the spikes. In Section 1.10, we exploit the high baseline to illustrate how adding a slow variable to the model can generate bursting behavior. Our tour of the Morris–Lecar model owes much to Rinzel and Ermentrout (1989) and many others, including Ellner and Guckenheimer (2006), Izhikevich (2007), Morris and Lecar (1981), and Sherman (2011).

Mathematically, a qualitative change in system behavior, such as the onset of spiking arises through a bifurcation. Different mechanisms for the onset of spiking correspond to different bifurcations. We work through each of these bifurcations carefully, as they typify the mechanisms for generating oscillations in two-dimensional systems, they can underlie mechanisms in higher dimensional systems, and they recur throughout the text.

Our interdisciplinary conversations have led to a route through the mathematical material that may seem unusual. We have not begun with local linear stability theory, because our experience suggests that, while many experimentalists have excellent intuition about rates of change at their fingertips, the abstraction of eigenvalues presents a road block. (This is a natural consequence of the typical mathematics requirements for a

biology degree.) We have chosen, instead, to harness the intuition about rates, and the visual intuition afforded by XPP, to develop an insight into the global nonlinear dynamics and bifurcations of the system. Only then we conclude with a discussion of the role eigenvalues play in determining local stability, and thereby signalling bifurcations. References are provided for the interested reader to learn more.

1.1 Introducing excitability

Action potentials: Decisive action and "information transportation". Cellular excitability is defined as the ability to generate an action potential (or spike): an explosive excursion in a cell's membrane potential (Figure 1.1). Its all-or-nothing aspect makes it decisive. Its propensity to propagate in space enables signal transmission in biological "wires" that are too small and electrically leaky to transmit a passive electrical signal over more than a millimeter or 2. Most cells have strong ionic gradients that are nearly, but imperfectly counterbalanced: a higher concentration of potassium ions (K^+) inside than out, versus higher sodium (Na^+), calcium (Ca^{++}) and chloride (Cl^-) concentrations outside than in. Higher "resting" permeabilities of the cell membrane to K and Cl result in a significant inside-negative *resting potential* (for largely historical reasons this is referred to as a *hyperpolarized* state). Action potentials are explosive excursions in the positive (*depolarizing*) direction from the resting potential, often reversing the polarity substantially (but still referred to as depolarizing).

The explosive mechanism uses positive feedback to produce a spatially regenerative event that propagates along a nerve axon, muscle fiber, or secretory cell's membrane. Positive feedback arises from the fact that the opening of either sodium (Na) or calcium (Ca) ion channels (small selective and gated pores in the cell membrane) is (1) promoted by depolarization and (2) leads to further depolarization, as Na or Ca ions enter through the opened channels. The explosive depolarization can propagate at rates anywhere from 1 to 200 m/s (Xu and Terakawa, 1999) depending on cell specifics. This is very slow compared to the passive spread of a voltage signal in a metal wire (on the order of the speed of light!). It is limited by the time required for channels to respond to voltage, together with the effects of membrane capacitance and leak. Nevertheless, it is much faster than any other form of chemical or biochemical signal propagation, and fast enough to support animal life, including the transmission of information over some 2 million miles of axons in the human body.

The explosive, roughly all-or-nothing nature of the action potential also serves as a decisively thresholded regulator of Ca entry. It thereby regulates many precisely timed and scaled cellular events, including

neurotransmitter and hormone secretion, muscle contraction, biochemical reactions, and even gene regulatory processes. Membrane voltage thus underlies rapid signal integration in the "biological computer," including the regulation of neuroendocrine function.

For a cell to recover from the excursion from negative resting potential and prepare to fire another action potential, repolarization has to occur. This is achieved by combatting the positive feedback with slightly delayed negative feedback, or feedbacks. An essentially identical mechanism of depolarization-triggered opening of ion channels as described for Na or Ca, but now involving a channel type that selectively conducts K, quickly restores the hyperpolarized state. In response, the Na- or Ca-channel gates can now relax back to the closed state (as do the K-channel gates), a process referred to as *deactivation*. In most cases, the K-channel restorative mechanism is backed up by the closing of a separate *inactivation* gate within the body of the Na or Ca channel, which would prevent prolonged depolarization (and flooding of Na or Ca into the cell) even without the K channel. Together these events speed repolarization, deactivation and *deinactivation* (the reversal of inactivation). The separability of these gating events provides raw material for very sophisticated and sometimes subtle differences in firing and consequent signal integration.

Action potential shape and timing in information processing. Synaptic transmission is well known to play important roles in information processing. The details of intrinsic excitability of neuroendocrine cells are at least as important as in neurons, and even more so in cells like those in the anterior pituitary that are not directly driven by synaptic inputs. Thus, the variety, subtlety and susceptibility to modulatory changes of ion channels underlying excitability are critical to the nuances of neuroendocrine signalling. See Hille (2001), Chapter 7 in Izhikevich (2007) and Figure 1.1. Details of the rising phase control threshold and rise time, and influence frequency. The details of repolarization, recovery, and preparation for subsequent signalling events are even more nuanced and diverse, as indicated by the enormous diversity of K channels (at least an order of magnitude greater than that of Na and Ca channels). Action potential threshold, differing between cells, and depending on recent events and modulatory factors within a cell, determines whether a response is transmitted or squelched. It also contributes, as do ensuing features of the action potential, to the encoding of the stimulus strength as firing frequency. Spike amplitude shapes calcium channel activation and calcium entry, as well as K-channel activation. These in turn sculpt ensuing features, and, especially through calcium influx, sculpt the transduction from electrical response to output, including, for example, transmitter, modulator, hormone release, or muscle contraction. The latency of the rising phase is critical to encoding or integration, and can serve as a temporal filter. So, too, can the timing of repolarization

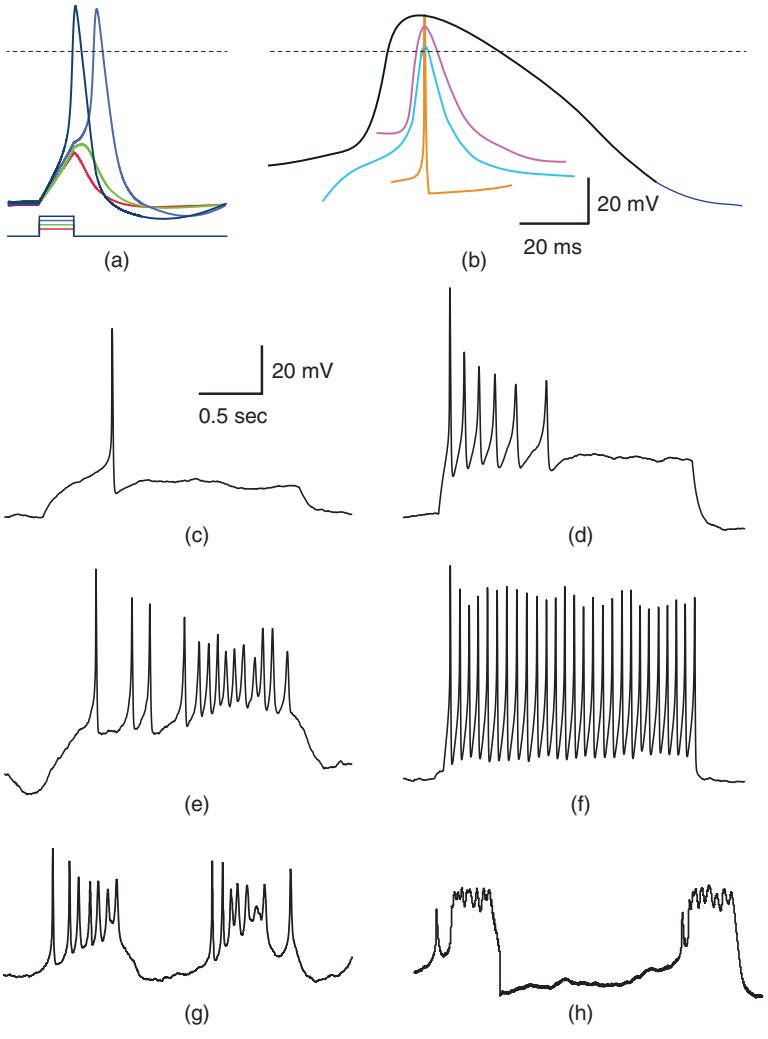

Figure 1.1 Variety of natural excitability. (a) Voltage responses of a mouse adrenal chromaffin cell to 10 ms current steps, recorded with whole-cell current clamp (McCobb Lab data). Action potential (AP) amplitudes were nearly invariant, and rise times varied modestly with stimulus amplitude. Voltage scale as in (b). (b) AP waveforms vary widely between cell types, ranging in duration from 180 μs for a purkinje cell (orange; Bean (2007)) to > 80 ms for a cardiac muscle AP (black). Shown for comparison are spikes from a barnacle muscle cell (blue; Fatt and Katz (1953)) and a chromaffin cell (purple; McCobb Lab). (c–f) Patterns of spikes elicited with sustained current steps vary even between mouse chromaffin cells (McCobb Lab). Cell (c) would not fire more than one spike, (d) fired a train with declining frequency, amplitude, and repolarization rate, (e), an irregular volley, and (f), a very regular train at high frequency. (g, h) Pituitary corticotropes fire spontaneous bursts with features that vary between bursts and between cells, including spike amplitudes and patterns, as well as burst durations (McCobb Lab). Scale bars in (c) apply to (c–h).

and recovery. These can confer a resonance on the system that makes it selectively responsive to timing of input, and potentially, as responsive to hyperpolarizing as depolarizing input. Timing and the interplay between the channel mechanisms together pattern the timing of spikes. They can also confer intrinsic firing, exemplified by the beautifully complex rhythms of burst firing. In addition to influencing reactivity to inputs, intrinsic firing makes a neuron a potential source of action (or maintenance or inaction). Together the dimensions of complexity and variability that have evolved in electrical signalling contribute enormously to the intelligence of biological systems, including (but not exclusive to) the brain function.

Dissecting action potential mechanisms with voltage clamp. Hodgkin and Huxley (1952) used the *voltage clamp* to dissect the action potential in the squid giant axon. (The axon is a milimeter or more in diameter, roughly 100 times the diameter of the largest human fibers). This clever device measures the opening and closing of ion channels, as follows: the voltage difference between the inside and outside of an axon is measured, and compared to a desired or "command" voltage. Any discrepancy between measured and command potentials is then immediately eliminated by injecting current into the axon through a second internal electrode. The amount of current required to clamp the voltage depends on the membrane conductance (inverse of resistance), and thus changes as ion channels open or close (see Figure 1.2). While useful for studying any channels, the voltage clamp is especially important for voltage-gated channels. By varying the voltage itself in stepwise fashion, Hodgkin and Huxley were able to prove that the membrane had conductances that were directly gated by voltage. Then by removing Na and K ions independently, they resolved distinct inward and outward components, and noted their dramatically different kinetics. The inward (Na) current responded more rapidly, but terminated quickly, while the outward (K) current was slower but persisted. Recognizing that this voltage sensitivity might provide the feedback underlying the action potential, they carefully measured voltage- and time-dependent features, including activation and deactivation of inward and outward components, and inactivation and deinactivation of the inward component. They then constructed a mathematical model and solved it numerically for the response to a stimulus, with the similarity between the theoretical voltage response and a recorded action potential supporting the view that they had explained the basic mechanism.

So why do we need to continue modeling action potentials and excitability? Hodgkin and Huxley (1952) predated the identification of ion channel proteins,

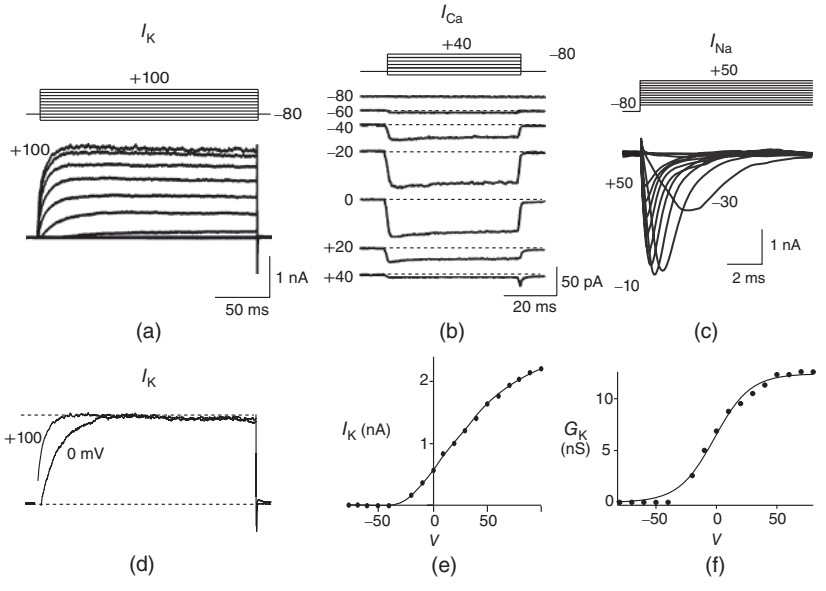

Figure 1.2 Voltage clamp data. (a, b, and c) Voltage-gated K, Ca, and Na currents, respectively, elicited with voltage steps in whole-cell voltage clamp mode applied to mouse chromaffin cells (McCobb Lab data). Outward currents are positive (upward), and inward currents are negative (downward). The K and Ca currents shown here exhibit little inactivation, though both types can inactivate in some chromaffin cells. The Na currents inactivate rapidly, and the current amplitude reverses sign when the test potential crosses the Na reversal potential. (d) K-current activation is faster at more depolarized potentials, as shown by normalizing the K currents at 0 and +100 mV from (a). (e) Current–voltage (*I–V*) plot for K currents from the cell in (a); peak current values are plotted against the corresponding test potential. (f) Conductance–voltage (*G–V*) plot; current values from (e) are divided by the driving force ($V_{test} - V_{reversal}$) and plotted against test potential. The *G–V* curve gives a summary of the voltage dependence of gating without the confounding effect of driving force.

but their results implied sophisticated voltage-sensing and gating nuances, and gave birth to structure-function analysis with unprecedented temporal resolution. Action potentials in barnacle muscle, another early preparation, were shown to depend on Ca rather than on Na influx (Keynes *et al.*, 1973). This laid the foundation for the Morris–Lecar model, in which one (excitatory) Ca current and one (repolarizing) K current interact to generate excitability (Morris and Lecar, 1981). Moreover, with glass electrodes enabling recordings in many more cell types, it became ever clearer that there was enormous variation on the general theme, begging further dissection. Every quantifiable feature of action potentials, from threshold to rise-time, duration, ensuing dip (*afterhyperpolarization*) and size, number, frequency, and pattern of additional action potentials elicited

by various stimuli could be shown to vary from cell to cell. It is now clear that this variety sculpts signal input–output relationships for neurons and networks in almost limitless fashion. Meanwhile, a vast array of ion channel genes, accessory proteins, and modulatory mechanisms contributing to excitability has been identified (Coetzee *et al.*, 1999; Dolphin, 2009; Hille, 2001; Jan and Jan, 2012; Jegla *et al.*, 2009; Lipscombe *et al.*, 2013; Zakon, 2012). A wealth of questions arise. How do structural elements and combinations encode functional nuances appropriate to physiological, behavioral, and ecological contexts in diverse animals? How did they arise through evolution? How they are coordinated in development? And how does event-sensitive plasticity contribute to adaptive modification of excitability-dependent computations? Relevant hypotheses clearly depend on theoretical dissection via mathematical modeling.

Why work with a model originating in barnacle muscle? Throughout the chapter, we will work with the Morris–Lecar model, which was originally developed for barnacle muscle and includes only two voltage-gated channel types (Ca and K), neither of which inactivates. Moreover, based on observations that showed the activation rate for the excitatory Ca current to be about 10-fold faster than that for the repolarizing K current and 20-fold faster than that for charging the capacitor (Keynes *et al.*, 1973), Morris and Lecar (1981) simplified the model even further, reducing dimension by treating the Ca-channel activation as instantaneous.

You may ask why a neurobiologist or endocrinologist should spend time on such a simple system, so obviously peripheral to sophisticated neural computation. Or how simplification and omission justify the trouble of learning mathematical "hieroglyphics". These questions raise the issue of what a mathematical model is good for. A powerful use of models is to help test hypotheses and design experiments about putative biological mechanisms underlying observed behaviors. To that end, minimal models, built from the ground up, allow for thorough dissection and attribution of mechanisms. For example, see Izhikevich (2007, Chapter 5) for a summary of six minimal models of excitability. After studying the Morris–Lecar model in this chapter, we hope that you will agree that what may at first look like an extremely limited system turns out to be capable of a surprisingly rich repertoire of waveforms and firing dynamics. Without studying such a minimal model, one might assume that more channel types or more complex gating mechanisms were needed to generate such a variety. After developing modeling confidence, it is easy to adjust parameters, or add inactivation, other channel types or gating mechanisms, as detailed in Chapter 2. The comparison between Morris–Lecar, Hodgkin–Huxley, and other model

behaviors then helps to clarify the interactive mechanisms at play, and the roles of specific terms and parameters.

The reduced dimension of the Morris–Lecar model also provides an excellent starting point for model analysis. It allows us to explore and dissect the model behavior in a two-dimensional *phase plane* (detailed in Section 1.4), where, with the help of graphical software, we can harness our visual intuition to understand the concepts and language of dynamical systems. The dynamical systems approach is extremely versatile, generalizing to more complex models and higher dimensions, and highlighting similarities among mechanisms in a wide range of applications. Throughout this volume, we will see how dynamical analysis of minimal models, designed with the scale and complexity of the specific neuroendocrine question in mind, yields new biological insights.

1.2 Introducing the Morris–Lecar model

The Morris–Lecar model is discussed in many texts in mathematical biology and theoretical neuroscience. See, for example, Ellner and Guckenheimer (2006), Ermentrout and Terman (2010), Fall *et al.* (2005), Izhikevich (2007), and Koch (1999).

What is in the Morris–Lecar model? The model structure is represented by the circuit diagram in Figure 1.3a (Morris and Lecar, 1981). A system of Ca and K gradients with selective conductances provides "batteries" defining equilibrium or reversal potentials. There is also a "leak" of undefined (probably composite) conductance, with a measurable reversal potential. For our purposes, the chemical gradients do not change appreciably: ion pumps and exchangers work in the background to ensure this. Currents applied through the current electrode travel in parallel across the capacitor and any open ion channels or other leaks. Internal and external solutions offer no resistance to flow, so that the voltage across the capacitor and resistors/conductors in the membrane is equivalent. Moreover, the system is assumed to be spatially uniform; voltage over the entire membrane changes in unison. This fits well with data from compact neuroendocrine cells (Bertram *et al.*, 2014; Liang *et al.*, 2011; Lovell *et al.*, 2004; Stojilkovic *et al.*, 2010; Tian and Shipston, 2000). The approach is also useful for membrane patches in most neuronal contexts. Spatial nonuniformity and spatio-temporal propagation of signals are not addressed here.

What makes this an "excitable" membrane and an interesting dynamical system, is (1) feedback: the proportion of channels open (for both Ca and K channels) depends on voltage and (2) reactions of the channel gates

to changes in voltage take time. Reaction rates also vary with voltage; but while this influences the voltage waveform, it is not essential for excitability.

Ion channel openings and closings are stochastic events, but their numbers are large enough that the currents associated with each type can be modeled as smooth functions. Thus, four variables interact dynamically:

- The voltage (transmembrane potential), V, typically in millivolts, mV.
- The proportion of open channels, M, for the voltage-gated Ca channel that drives the rising phase of the action potential. Since M is a proportion, it ranges between 0 and 1, and has no units.
- The proportion of open channels, W, for the voltage-gated K channel that terminates the action potential. Like M, W is a proportion, so ranges between 0 and 1.
- Time, t, the independent variable, typically in milliseconds, ms.

Again, the dependent variables are functions of one another; they interact, and do so with time dependence. The rules by which they interact are translated into differential equations, as discussed below.

What is a differential equation? The only mathematical background we assume is that you have taken a calculus course sometime in the past (perhaps long ago) and remember (perhaps dimly) that the *derivative* represents instantaneous rate of change, or the slope of a graph. For example, Figure 1.1 shows several graphs of voltage, $V(t)$ versus time. Consider the detailed action potentials shown in Figure 1.1b. During the rising phase of each action potential, the slope of the graph is positive. So the derivative, $\frac{dV}{dt}$, is positive. This is just another way of saying that V is increasing or depolarizing. During the hyperpolarizing (decreasing) phase of each action potential, the graph is heading "downwards," with a negative slope, so $\frac{dV}{dt} < 0$. At the peak of each action potential, a line tangent to the graph would be horizontal, with zero slope. So $\frac{dV}{dt} = 0$ as the graph turns from increasing to decreasing. Similarly, $\frac{dV}{dt} = 0$ as the graph turns from decreasing to increasing.

(1.2.1) This is where the interactive part of the tutorial begins. This first exercise is designed to help cement the concepts of slope and derivative, and does not require any software. Choose one of the graphs in Figure 1.1 and track $\frac{dV}{dt}$ as you move along the graph. When is $\frac{dV}{dt}$ positive? When is it negative? How many times is it zero? When is $\frac{dV}{dt}$ greatest? When is it most negative? Try sketching the graph of $\frac{dV}{dt}$ below your graph of $V(t)$ (it helps to have the time axes lined up).

A *differential equation* is just an equation with a derivative in it somewhere. Equation (1.1) is a differential equation relating the rate of change

of voltage to the currents flowing through the cell membrane. The differential equation does not tell us about V directly, in the sense that it is not of the form

$$V(t) = \text{"something"}$$

But if we can measure the value of V at one *initial* moment in time, Equation (1.1) tells us how V will change, so that we can use it to predict all future values of $V(t)$. Adding up all the incremental changes in V over time is called *numerical simulation*. It can be hard to do by hand, but is a job well suited to a computer. This is one of the reasons that mathematical modeling in biology has flourished with the computer revolution of recent decades, and why this tutorial is designed to be interactive, using the numerical simulation software XPP (Ermentrout, 2012).

A word of warning: the derivative is a fundamental concept in math ematics, so has earned many names; $\frac{dV}{dt}$ ("dV by dt"), V' ("V prime"), and $\dot{V}$ ("V dot") are all equivalent in this context, and not to be confused with plain V.

The differential equation for voltage change over time. According to Kirchoff's current law, if a current I is applied across the membrane (through an electrode, say), it is balanced by the sum of the capitative and ionic currents:

$$I = C\frac{dV}{dt} + I_{\mathrm{Ca}} + I_{\mathrm{K}} + I_{\mathrm{L}}$$

If there is no applied current, then $I = 0$. Here, I_{Ca} and I_{K} denote the Ca and K currents respectively; I_{L} denotes a leak current (a voltage independent current that may or may not be selective); C denotes the capacitance, and $C\frac{dV}{dt}$ represents the capacitive current. The fact that capacitive current is proportional to how quickly voltage changes $\left(\frac{dV}{dt}\right)$ is what makes this a differential equation. Rearranging to bring the derivative to the left-hand side,

$$C\frac{dV}{dt} = I - I_{\mathrm{Ca}} - I_{\mathrm{K}} - I_{\mathrm{L}}$$

Thus,

$$C\frac{dV}{dt} = I - g_{\mathrm{Ca}}M(V - V_{\mathrm{Ca}}) - g_{\mathrm{K}}W(V - V_{\mathrm{K}}) - g_{\mathrm{L}}(V - V_{\mathrm{L}}) \tag{1.1}$$

where the ionic currents are modeled by

$$I_{\mathrm{Ca}} = g_{\mathrm{Ca}}M(V - V_{\mathrm{Ca}}) \tag{1.2}$$

$$I_{\mathrm{K}} = g_{\mathrm{K}}W(V - V_{\mathrm{K}}) \tag{1.3}$$

$$I_{\mathrm{L}} = g_{\mathrm{L}}(V - V_{\mathrm{L}}) \tag{1.4}$$

Let us walk through these equations term by term, to understand the notation, and how the ionic currents are represented. To fix ideas, consider the K current. In Equation (1.3), I_K is modeled as the product of:

- The maximal K conductance, g_K, that can be measured at any voltage (see Figure 1.2).
- The K-channel activation variable, W, which changes over time (so is written $W(t)$, or W for short). There is no K-channel inactivation in the model, so, relative to maximal conductance, $W(t)$ represents the proportion of K channels that are open at time t, and the instantaneous probability that an individual K channel is in its open state. In other words, $W(t)$ represents the normalized K conductance at time t (taking values between 0 and 1), and $g_K W(t)$ represents the absolute K conductance. Expressions for the voltage dependence and kinetics of W are formulated in Equations (1.6), (1.9), and (1.10).
- The driving force, $(V - V_K)$, on K current through the K channels. This is the difference between V of the moment and V_K, the K reversal potential. The larger the difference, the larger the driving force; and as V changes over time, the driving force changes accordingly.

Thus, Equation (1.3) is simply a mathematical translation of the fact that K current is given by K conductance multiplied by K driving force. Clear translation between the biology and the mathematics is at the heart of mathematical modeling.

The Ca and leak currents are treated similarly, with the Ca-channel activation variable denoted by M in Equation (1.2). Equation (1.4) for the leak current looks slightly different, because leak conductance is assumed to be independent of voltage, so it does not need an activation variable. Thus, the leak has constant conductance, g_L. In this tutorial, we set the conductances at $g_{Ca} = 4$, $g_K = 8$ and $g_L = 2$ (see Table 1.1).

(1.2.2) In this exercise, let us think about the impact of the K current on V, to help understand the signs in Equation (1.1). If $V > V_K$, is I_K positive or negative? It helps to remember that g_K and W are both positive. You should find that I_K is positive. So, when you check the signs in Equation (1.1), you see that the K current contributes *negatively* to $\frac{dV}{dt}$. That is, the K current promotes change in the negative direction. In the absence of other currents, what impact would this have on V? Would it increase V or decrease V? So, is the K current driving V towards V_K, or away from V_K? (Remember that we started by assuming $V > V_K$.)

(1.2.3) What happens if $V < V_K$? Explain how the K current drives V towards V_K in this case, too.

The reversal potential for a purely selective channel is equal to the Nernst equilibrium potential for the ion carrying the current. For a current representing multiple permeabilities (such as leak), the reversal potential is calculated using the Goldman–Hodgkin–Katz equation if the relative permeabilities and ionic gradients are known, or measured in voltage clamp if

the current species can be isolated (Hille 2001). In this tutorial, we set the reversal potentials at $V_{Ca} = 120$ mV, $V_K = -84$ mV, and $V_L = -60$ mV (see Table 1.1.)

Looking back at Equation (1.1), we can think of the three ionic currents competing with each other and with the applied current, each trying to drive V to its own reversal potential as in Exercises 1.2.2 and 1.2.3. Over the course of an action potential, the different voltage dependence of Ca- and K-channel gating changes the relative sizes of M and W, allowing different terms in Equation (1.1) to dominate. When the Ca term dominates, V is driven toward the high Ca reversal potential and the cell depolarizes. And when the K term dominates, V is driven back down toward the low K reversal potential and the cell hyperpolarizes (see Figure 1.4a).

The voltage dependence of steady-state conductance. K-channel activation, W, is assumed to have kinetics and voltage dependence. Both aspects are measured using the voltage clamp, as illustrated in Figure 1.2. In these experiments, the voltage is stepped instantaneously to each of a series of test voltages and held there, while the current reaches a new steady state (Figure 1.2a). Arrival at the steady state is not instantaneous, but defines the kinetics of channel activation, which is itself voltage dependent (Figure 1.2d). We return to the kinetics presently.

The amount of current at the steady state for a test voltage reflects the conformational stability of open states of the K channel; the greater the stability, the more channels open and the greater the conductance. To characterize the voltage dependence of steady-state conductance, the steady-state values of current are first plotted against test voltage to give the current–voltage (I–V) plot (Figure 1.2e). Since the measured current is assumed to be the product of driving force and conductance, the current is divided by the driving force to give the conductance–voltage (G–V) plot (Figure 1.2f). To estimate the maximal conductance, g_K, the G–V curve is fit with a Boltzmann function (Figure 1.2f), then g_K is given by the maximal value, or upper asymptote, of the Boltzmann curve. The Boltzmann function is then normalized (divided) by g_K to yield the proportion, $W_\infty(V)$, of (activatable) channels that are open at the steady state, as a function of V.

Equations (1.5) and (1.6) define the steady-state open probabilities, $M_{\infty(V)}$ and $W_{\infty(V)}$, for the Ca and K channels, respectively, in our Morris–Lecar model (see Figure 1.3b):

$$M_\infty(V) = \frac{1}{1 + e^{-2(V-V_1)/V_2}} = 0.5\left(1 + \tanh\left(\frac{V - V_1}{V_2}\right)\right) \tag{1.5}$$

$$W_\infty(V) = \frac{1}{1 + e^{-2(V-V_3)/V_4}} = 0.5\left(1 + \tanh\left(\frac{V - V_3}{V_4}\right)\right) \tag{1.6}$$

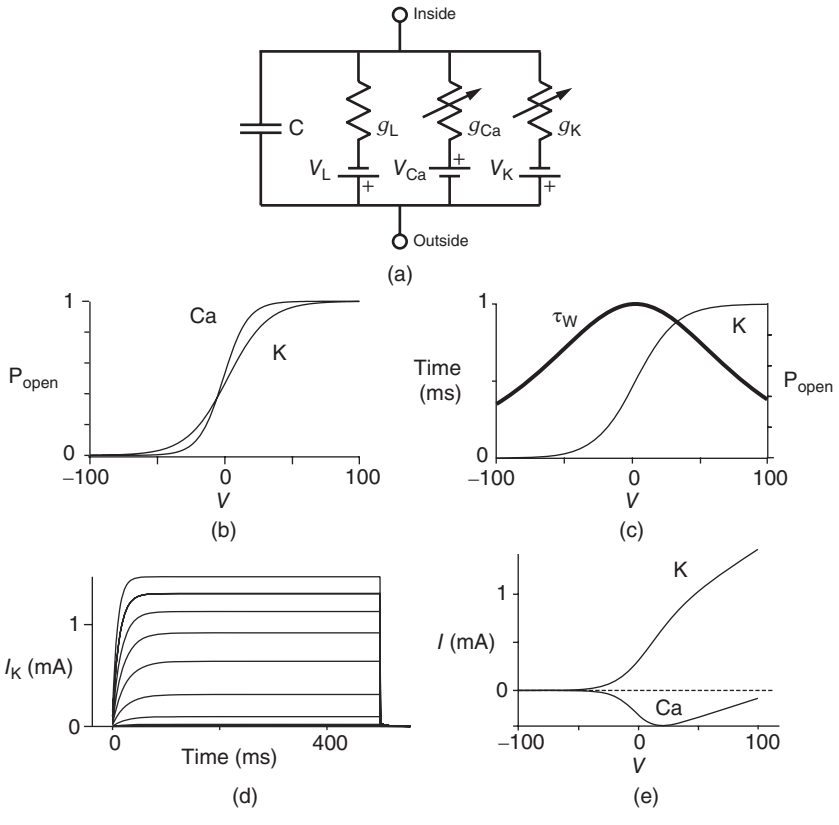

Figure 1.3 Morris–Lecar model. (a) Equivalent electrical circuit representation of the Morris–Lecar model cell. Membrane capacitance is in parallel with selective conductances and batteries (representing driving forces arising from ionic gradients). Arrows indicate variation (with voltage) for Ca and K conductance. (b) Normalized G–V curves, W_∞ and M_∞, assumed for model K and Ca conductances, respectively. (c) The kinetics of voltage-dependent activation of K channels is also voltage dependent, with the normalized time constant, τ_W, assumed to peak (i.e., channel gating slowest) at the midpoint of the G–V curve, where channel conformational preference is weakest. (d) Simulated voltage clamped K currents at 20 mV increments up to V=100 mV. Voltage clamp simulated in XPP by removing the equation for dV/dt and, instead, setting V as a fixed parameter. (e) Model I–V plots for K and Ca currents. Different reversal potentials for the two conductances ($V_K = -84, V_{Ca} = 120$ mV) make the current traces look very different, despite similar activation functions in (b). (b)–(e) Use Hopf parameter set.

In the next exercises, we will graph $W_\infty(V)$ to cement intuition for the role of V_3 and V_4. $M_\infty(V)$ is similar. In Exercise 1.2.7, we will confirm that the two different forms of the equations are, indeed, equal. The exercises are written with the online graphing calculator *Desmos* in mind, but any graphing calculator will do. We choose Desmos because it is fun to work with, and for the ease of setting up sliders to explore the way parameters

shape the graph. See Table 1.1 for the values of V_1, V_2, V_3, and V_4 used in later sections of this tutorial.

(1.2.4) Open Desmos in a browser (www.desmos.com). You enter functions in the panel on the left, and watch them appear on the axes on the right. For example, click on the left panel, and type in $y = e^x$. You should see the familiar exponential function appear. Now click on the next box on the left, and enter $y = e^{(x-c)}$. Click on the "button" to accept the offer to add a slider for c. Slide the value of c (by hand, or by clicking the "play" arrow) and watch your graph shift to the left or right accordingly. Now, try $y = d + e^{(x-c)}$. You can add a new slider for d. What is the effect of sliding d? Notice how the old c slider now works for both the functions. You can temporarily hide a graph by clicking on the colored circle next to its equation, or permanently erase it by clicking on its gray X. There is also an edit button to explore.

(1.2.5) As we have seen, Desmos uses x and y for variables, and single letters for other parameters. So, to graph $W_\infty(V)$, you will need to re-write Equation (1.6) with x playing the role of V, y playing the role of W_∞, a playing the role of V_3 and b playing the role of V_4. In other words, working with the Boltzmann form of Equation (1.6) first, enter

$$y = \frac{1}{1 + e^{(-2(x-a)/b)}} \tag{1.7}$$

(being careful with your parentheses!), and accept the sliders for a and b. You should see a typical (normalized) G–V curve ranging between 0 and 1, as shown in Figures 1.2f, 1.3b, and 1.3c. Slide a and b to see what role they play in shaping the curve. You can change the limits of the sliders if you like. For example, click on the lower limit of b and set it to zero, to keep b positive.

(1.2.6) Translating back to the language of Equation (1.6), confirm that V_3 is the half-activation voltage of W_∞, and V_4 determines the "spread" of W_∞. As V_4 increases, the spread increases. In other words, as V_4 increases, the slope at half-activation decreases. In fact, differentiating Equation (1.6) at $V = V_3$ shows that the slope at half-activation is given by $\frac{1}{2V_4}$. Confirm this with Desmos, by graphing the line $y = \frac{1}{2} + \frac{1}{2b}$ (which has slope $\frac{1}{2b}$) together with Equation (1.7), setting $a = 0$, and sliding b.

(1.2.7) Use Desmos to plot

$$y = 0.5\left(1 + \tanh\left(\frac{x-a}{b}\right)\right) \tag{1.8}$$

and confirm that this second form of Equation (1.6) is equivalent to the first. In other words, it has exactly the same graph. This second form is also commonly used, and you will see it in the XPP code provided. If you are unfamiliar with the hyperbolic tangent function, $\tanh x$, develop your intuition by building up the graph of Equation (1.8) in parts. First

graph $y = \tanh x$, then $y = \tanh(x - a)$, etc. (Recall that the more familiar $\sin x, \cos x$, and $\tan x$ are defined using a point on the unit circle $x^2 + y^2 = 1$. The hyperbolic functions $\sinh x$, $\cosh x$, and $\tanh x$ have analogous definitions using a point on the hyperbola $x^2 - y^2 = 1$.)

Voltage-dependent kinetics of voltage gating. Now we return to the kinetics of K-channel gating, governing the rate of approach to the steady state. The channels are trying to reach the steady state for conductance at a particular voltage, but during the process the voltage is typically changing. As a result, the channels are always playing catch-up. Moreover, the rate at which the channels respond to voltage is itself a function of voltage. These kinetics are modeled by the differential equation

$$\frac{dW}{dt} = \frac{\phi}{\tau_W(V)}(W_\infty(V) - W) \tag{1.9}$$

Here, ϕ and $\tau_W(V)$ are both positive, and together define the time scale (or time constant) of K kinetics. The voltage dependence of the time scale is captured by the equation for $\tau_W(V)$

$$\tau_W(V) = \frac{1}{\cosh((V - V_3)/2V_4)} \tag{1.10}$$

See Figure 1.3c. We will develop intuition for Equations (1.9) and (1.10) in the following exercises. See Table 1.1 for the values of ϕ, V_3, and V_4 used in later sections of this tutorial.

(1.2.8) First let us focus on the $(W_\infty(V) - W)$ term in Equation (1.9). It is reminiscent of the $(V - V_K)$ term in Equation (1.3), and can be analyzed in a similar way. Recall that V and W change over time. So, at a given time t, V and W will have values $V(t)$ and $W(t)$. What happens if, at time t, $W(t) > W_\infty(V(t))$? Will W increase or decrease in the next increment of time? Remember that ϕ and $\tau_W(V)$ are both positive. So, if you keep track of the signs, you should find that if $W(t) > W_\infty(V(t))$, then $dW/dt < 0$, so W is driven down, toward $W_\infty(V(t))$.

(1.2.9) What happens if $W(t) < W_\infty(V(t))$? Explain how the conductance is driven towards steady state in this case, too. As time marches on, V changes. So the voltage-dependent steady-state conductance, $W_\infty(V)$, also changes. Thus, the $(W_\infty(V) - W)$ term in Equation (1.9) ensures that W adjusts course accordingly, in its tireless game of catch-up.

(1.2.10) Now, let us focus on $\tau_W(V)$ to prepare us for understanding its role in Equation (1.9). Use Desmos to graph $\tau_W(V)$, as shown in Figure 1.3c. Recall that you will need to rewrite the equation for $\tau_W(V)$ with x playing the role of V, y playing the role of τ_W, and single letters playing the role of V_3 and V_4. For example, you could graph

$$y = \frac{1}{\cosh((x - a)/2b)} \tag{1.11}$$

with sliders for a and b. Here, $\cosh x$ stands for hyperbolic cosine, the analog of cosine for the hyperbola. If you are unfamiliar with hyperbolic cosine, then build up Equation (1.11) in parts: first graph $y = \cosh x$, then $y = \cosh(x - a)$, etc. What role does a play in the graph of Equation (1.11)? What role does b play? What is the maximum value of τ_W? What is the minimum value? Translating this back to the language of Equation (1.10), you should find that $\tau_W(V)$ reaches a peak value of 1 at $V = V_3$, and decays down to zero on either side of V_3. The rate of decay is governed by V_4: the greater the value of V_4, the greater the "spread" of τ_W.

(1.2.11) Recall that V_3 and V_4 are also the shape parameters for $W_\infty(V)$. Use Desmos to plot the graph of $W_\infty(V)$ on the same axes as your graph of $\tau_W(V)$ (see Figure 1.3c). Use a to represent V_3 in both equations, and b to represent V_4. Then, when you slide a and b, you can see their effect on both equations simultaneously. What do you notice? τ_W and W_∞ have similar spreads, and τ_W has its maximum at the half-activation voltage of K conductance.

(1.2.12) Now, look back at Equation (1.9). Does W change faster when $\tau_W = 1$ or when $\tau_W = 0.1$? In other words, does W change faster at half-activation, or far from half-activation? Does that make sense?

Recapping, Equations (1.9) and (1.10) model the voltage-dependent kinetics of K^+ conductance. The time constant $\frac{\tau_W(V)}{\phi}$ governs the rate at which W catches up with the ever-changing $W_\infty(V)$. The kinetics are slowest around the half activation voltage where the probabilities of K^+ channel opening or closing balance.

Fast calcium kinetics reduce the dimension of the model. Equations similar to (1.9) and (1.10) could be used to model the kinetics of Ca conductance. However, as described in Section 1.1, Morris and Lecar (1981) used the time-scale separation observed between the Ca and K kinetics to reduce the dimension of their model. Instead of including an additional differential equation to follow the very fast approach of Ca conductance to its steady state, they made the assumption that Ca-channel activation occurs immediately, relative to the time scale of K kinetics. In other words, they assume that Ca activation, M, is always "caught-up" to $M_\infty(V)$. So, $M_\infty(V)$ can be substituted for M in Equation (1.1), yielding Equation (1.12).

Summarizing. The Morris–Lecar model is given by the system of two coupled nonlinear differential equations

$$C\frac{dV}{dt} = I - g_{Ca}M_\infty(V - V_{Ca}) - g_K W(V - V_K) - g_L(V - V_L) \qquad (1.12)$$

$$\frac{dW}{dt} = \frac{\phi}{\tau_W(V)}(W_\infty(V) - W) \qquad (1.13)$$

where

$$M_{\infty}(V) = 0.5\left(1 + \tanh\left(\frac{V - V_1}{V_2}\right)\right) \tag{1.14}$$

$$W_{\infty}(V) = 0.5\left(1 + \tanh\left(\frac{V - V_3}{V_4}\right)\right) \tag{1.15}$$

$$\tau_W(V) = \frac{1}{\cosh((V - V_3)/2V_4)} \tag{1.16}$$

The variables, parameters, and parameter values we use are summarized in Table 1.1.

Table 1.1 Variables and parameter values used.

Variable or parameter	Definition	Units	Hopf values	SNIC values	Homo values
t	Time	ms			
$V(t)$	Membrane voltage at time t	mV			
$W(t)$	Proportion of K channels open at time t				
$M_{\infty}(V)$	Proportion of Ca channels open at steady state at voltage V				
$W_{\infty}(V)$	Proportion of K channels open at steady state at voltage V				
I	Applied current*	$\mu A\ cm^{-2}$			
C	Capacitance*	$\mu F\ cm^{-2}$	20	20	20
V_{Ca}	Ca reversal potential	mV	120	120	120
V_K	K reversal potential	mV	−84	−84	−84
V_L	Leak reversal potential	mV	−60	−60	−60
g_{Ca}	Maximal Ca conductance*	$mS\ cm^{-2}$	4	4	4
g_K	Maximal K conductance*	$mS\ cm^{-2}$	8	8	8
g_L	Leak conductance*	$mS\ cm^{-2}$	2	2	2
V_1	Voltage at half-activation of Ca channels	mV	−1.2	−1.2	−1.2
V_2	Spread (steepness $^{-1}$) of $M_{\infty}(V)$	mV	18	18	18
V_3	Voltage at half-activation of K channels	mV	2	12	12
V_4	Spread (steepness $^{-1}$) of $W_{\infty}(V)$	mV	30	17	17
ϕ/τ_W	Rate constant for K-channel kinetics	ms^{-1}			
$\tau_W(V)$	Voltage dependence of K-channel kinetics	ms			
ϕ	Rate constant for K-channel kinetics at half-activation voltage		0.04	0.04	0.22

*Throughout the tutorial, we suppress the cm^{-2} on current, capacitance, and conductance.

What does the model tell us? Now, we have equations for how V and W change! In the rest of the tutorial, we use numerical simulation and graphical analysis to gradually uncover the richness of behavior the minimal mechanisms included in this model cell can exhibit.

The model is autonomous. Notice that the independent variable, time, does not appear explicitly in the right-hand sides of Equations (1.12)–(1.16). So the system is *autonomous*, or self-governing, meaning that the rates of change, $\frac{dV}{dt}$ and $\frac{dW}{dt}$ depend only on the state of V and W, and not on when they achieve that state. In Section 1.4, we will see how this autonomous structure is key to the phase-plane approach used throughout the text.

1.3 Opening XPP and triggering an action potential

From here on, you will need a dynamical systems software package to work the interactive exercises. The main tools used in this tutorial are: (1) numerical integration of systems of two and three differential equations, and plotting solutions against time, and (2) phase-plane plots and calculations for systems of two differential equations, including trajectories, direction fields, nullclines, equilibria, limit cycles, and eigenvalues. We will define these terms as we come to them.

There are many good software packages available for simulating differential equations, each with its own strengths and weaknesses. We have written this tutorial to work directly with XPP (also called XPP-Aut), by Bard Ermentrout (2012). We have chosen XPP for several reasons. It is freely available, widely used in the computational neuroendocrine community, and works on many platforms, including Mac, Windows, and Linux machines, all with the same menu system and graphical user interface. We find that it has a good balance of computational power, user friendliness, and modeling freedom. The combination of two-dimensional phase-plane graphics and the capability of simulating higher dimensional models is particularly useful, especially if your goal is to develop more complex models of your own, involving several coupled differential equations. XPP can also simulate many types of differential equation, and a wide range of examples from biology, chemistry, and physics are included with the download.

There are also XPP apps for the iPad and iPhone. The interface is different for these apps, since it makes use of the touch-sensitive screen. Thus, to work this tutorial on an iPad or iPhone, you will need to learn the interface and modify our menu instructions. Similarly, if you prefer a different software package, it should be straightforward to

translate the exercises accordingly. For example, PPLANE (MATLAB or Java based, http://math.rice.edu/ dfield) and Berkeley Madonna (www.berkeleymadonna.com) both have user friendly two-dimensional phase-plane graphics. Or you may prefer the independence of Matlab (www.mathworks.com), R (http://www.r-project.org), or Mathematica (http://www.wolfram.com/mathematica). See the online supplementary materials to Ellner and Guckenheimer (2006) for Matlab and R-tutorials, and R-based PPLANE.

Download XPP. At the time of writing, the following steps work to download the Mac, Windows, or Linux versions of XPP.

- Visit Bard Ermentrout's XPP-Aut page at: http://www.math.pitt.edu/bard/xpp/xpp.html There is online documentation, an interactive tutorial, and much more. Read the information for your platform below the *DOWNLOAD* link, then click on *DOWNLOAD*.
- Go to *Assorted Binaries*, then *Latest* to find the latest binary file for your platform. Mac versions are "dmg" files with "mac" or "osx" in the title somewhere, windows versions are "zip" files with "win" in the title somewhere.
- Download a version for your platform, then open the file *install.pdf*. Carefully follow the instructions that tell you where to put the files, how to download an "X server," if necessary, and how to fire up XPP. (If you run into trouble trying to quit XPP, look ahead a couple of pages to the paragraph headed *Essential XPP tips.*)

ODE files. XPP is a tool for simulating differential equations. It reads the equations from an *ODE file* written by the user. There is a lot of helpful information about the structure of ODE files, and a wealth of examples, on the XPP website. Example ODE files are also included in the files downloaded with XPP, together with a manual (*XPP_doc*) and a succinct summary of commands (*XPP_sum*) in PDF and postscript (ps) formats. XPP was written for applications to neuroscience, and the manual and online tutorial use neural models throughout. It is well worth learning to read and write ODE files, as it gives you control over the nuances of the model, and the freedom to experiment with new models of your own. The components of the ODE file given below will be explained as we work with it in XPP.

Download the ODE file for this tutorial. For the interactive exercises, you will need the file BridgingTutorial-MLecar.ode reproduced below. Electronic copies are available on the website for this volume and from the authors. We recommend downloading an electronic copy, to save yourself the trouble of re-typing it and, more importantly, the possibility of mis-typing.

As stated in the XPP manual: "ODE files are ASCII readable files that the XPP parser reads to create machine usable code." This means that it is important to use a plain text editor for ODE files, because complex editors (such as word) add invisible extra characters to your document that render it unreadable to XPP. Use an editor like Textedit (on a Mac) or NotePad or WordPad (in Windows). Be sure to save the file as plain text such as ASCII, or UTF-8.

```
# BridgingTutorial–MLecar.ode
# From 'Bridging Between Experiments and Equations' by McCobb and Zeeman
# Adapted from online examples by Bard Ermentrout and by Arthur Sherman

# differential equations
dV/dt = (I – gca*Minf(V)*(V–Vca) – gk*W*(V–Vk) – gl*(V–Vl))/C
dW/dt = phi*(Winf(V)–W)/tauW(V)

# functions
Minf(V)=.5*(1+tanh((V–V1)/V2))
Winf(V)=.5*(1+tanh((V–V3)/V4))
tauW(V)=1/cosh((V–V3)/(2*V4))

# default initial conditions
V(0) = −60
W(0)=0

# default parameters
param I=0,C=20
param Vca=120,Vk=–84,Vl=–60
param gca=4,gk=8,gl=2
param V1=–1.2,V2=18

# uncomment the parameter set of choice
param V3=2,V4=30,phi=.04
# param V3=12,V4=17,phi=.04
# param V3=12,V4=17,phi=.22

# choose a parameter set using '(F)ile' then '(G)et par set' in XPP menu
set hopf  {Vca=120,Vk=–84,Vl=–60,gca=4,gk=8,gl=2,C=20,V1=–1.2,V2=18,V3=2,  V4=30,phi=.04}
set snic  {Vca=120,Vk=–84,Vl=–60,gca=4,gk=8,gl=2,C=20,V1=–1.2,V2=18,V3=12,V4=17,phi=.04}
set homo {Vca=120,Vk=–84,Vl=–60,gca=4,gk=8,gl=2,C=20,V1=–1.2,V2=18,V3=12,V4=17,phi=.22}

# track some currents and conductances
aux Ica = gca*Minf(V)*(V–Vca)
aux Ik = gk*W*(V–Vk)
aux Il = gl*(V–Vl)
aux CaCond = gCa*Minf(V)
aux KCond = gk*W
aux POpenCa = Minf(V)
aux POpenK = W

# Open XPP with (t,V) voltage–trace window or (V,W) phase–plane window.
@ xp=t,yp=V,xlo=0,xhi=200,ylo=–80,yhi=50
# @ xp=V,yp=W,xlo=–75,xhi=70,ylo=–0.2,yhi=1

# some numerical settings
@ dt=.25,total=200,bounds=10000,maxstore=15000

done
```

Reading the ODE file. Lines beginning with a # symbol are not read by XPP. They can be used for comments, or to make choices between options by inactivating the unwanted options.

(1.3.1) Find the differential equations and associated functions in *BridgingTutorial-MLecar.ode*, and check that they agree with Equations (1.12)–(1.16). The notation is slightly different in XPP, because there are fewer symbols available and no subscripts, but the translation from Equations (1.12)–(1.16) is fairly straightforward. For example, *Minf(V)*, *Winf(V)*, *tauW(V)*, and *phi* correspond to $M_\infty(V), W_\infty(V), \tau_W(V)$, and ϕ, respectively.

(1.3.2) Confirm that the parameter values listed in the ODE file agree with those in Table 1.1.

Initial conditions. Recall from Section 1.2 that the differential equations for V and W tell us the rate of change of V and W. So, if we know the values of V and W at one *initial* moment in time, we (or preferably XPP) can numerically predict the future values of $V(t)$ and $W(t)$ by adding on the incremental changes over time. Thus, in order to simulate the time course of V and W, XPP needs *initial conditions* $V(0)$ and $W(0)$.

(1.3.3) Find the default initial conditions in the ODE file. What does the initial condition $W(0) = 0$ tell you about the K channels?

(1.3.4) The initial membrane voltage is $V(0) = -60$. What does this tell you about the Ca channels? Hint: Use the equation for the voltage dependence of Ca-channel gating (Equation (1.14)), with the parameter values from the ODE file (see also Figure 1.3b).

Notice, again, the difference in the way Ca and K channels are treated in the model. The assumption of "instantaneous" kinetics of Ca-channel gating means that the state of the Ca channels at any given time can be deduced directly from the membrane voltage at that time. In particular, the initial state of the Ca channels follows from that of the membrane voltage, as in Exercise 1.3.4. By contrast, the slow response of K channels to changing voltage is tracked by $W(t)$, which, in turn, depends on their initial state, $W(0)$.

(1.3.5) Confirm that the applied current, I, is set to a default value of zero in the ODE file. In the absence of applied current, and with the default initial conditions, how do you expect this cell to behave?

The rest of the ODE file will be explained as we work with XPP. For more information, see the XPP manual *XPP_doc* (included with the download and available online (Ermentrout, 2012)).

Opening XPP. Methods for firing up XPP depend on the platform you are using and are described in the file *install.pdf* included with the download. In all cases, XPP has a console window, and is fired up from the console using an ODE file. On a Mac and Windows computer, the install instructions describe how to set up a shortcut to the XPP console. XPP can be started by dragging an ODE file onto the icon, or into the open console window. On a Linux computer, the install instructions describe how to set up the path and fire up ODE files from the command line (the terminal window then functions as the console). The console reports errors and other useful information.

(1.3.6) Fire up XPP using the ODE file *BridgingTutorial-MLecar.ode*. The console will report XPP's progress on reading the ODE file and, if all is well, an XPP command window will open up. The command window includes a graphics window, a menu down the left-side buttons and a command line along the top, and sliders along the bottom. If the menu and sliders are overlapping, enlarge the window by dragging the bottom right corner. Let us graph the voltage time course of our model cell. Click on the ICs button at the top of the command window. A small window should open, showing the initial condition $V = -60$ and $W = 0$. Click *Go*. An unremarkable voltage trace appears on the graph, showing a cell at rest, close to $V = -60$. Is this what you expected?

Essential XPP tips. We will use XPP to trigger action potentials, explore and dissect the model behavior, and learn some of the concepts and language of dynamical systems. But first a few essential tips to help give you immediate XPP independence.

- Quitting XPP. There are several ways to quit XPP, none of them quite obvious. In the command window menu, click *File* then *Quit* in the submenu, then *Yes* on the tiny pop-up window. Alternatively, depending on your operating system, you may be able to click *Cancel* on the console (bottom right), then click *Quit* in the same place.
- To close a pop-up window, use the *close* button within the window. The usual way of closing windows (e.g., red button on a mac) may not work.
- The capital letter in the name is the shortcut to each menu item. Within each submenu, there are similar shortcuts, shown in parentheses. For example, typing *FQY* is a shortcut for quitting XPP. Henceforth, we will show the short cuts in parentheses.
- When you hover over a menu item with the mouse, a brief description is given in the skinny text line along the bottom of the command window.
- Sometimes you need to press the *escape* key to escape the mode you have put XPP into. For example, the *(N)umerics* menu is unlike the others: if you enter it, you need to press *escape* to exit.

- Sometimes XPP needs your input before it can run your command. For example, if you click on *(X)i* versus *t* in the menu, it may appear that nothing has happened. In fact, the skinny command line along the top of the command window is asking you which variable you want to plot against time, *t*. Enter your choice (e.g., *W*), then press return.
- So, if XPP seems unresponsive, check to see if it is asking a question in the command line or in a tiny pop-up window (possibly hidden behind other windows). If not, try pressing escape a few times.
- Some menu items only apply to some types of graph. For example, the *(D)ir. field/flow* menu only works when you are plotting two dependent variables against each other (e.g., *V* versus *W*, see Section 1.4). Otherwise, nothing happens when you try it.
- Succinct information about all the main menu and submenu commands is listed in the manual *XPP_doc* that is downloaded with XPP, and in the *Online Documentation* on the XPP homepage (Ermentrout, 2012).

Triggering an action potential. Returning to our model cell, imagine applying a short pulse of positive current, as in a current clamp experiment designed to characterize the cell's excitability. During the pulse, the membrane voltage will rapidly depolarize (increase), with the amount of depolarization depending on the magnitude and duration of the applied current. The K channels will, in turn, respond to the voltage change, but on a slower time scale. A useful way to think about this, from the modeling point of view, is that the brief stimulus has the effect of resetting the initial values of *V* and *W*, where the word "initial" now refers to the moment of termination of the stimulus (initiation of the post-stimulus response). In other words, we can think of the initial values of *V* and *W* as reflecting the recent history of the cell. In the case of our stimulus pulse, if it is very brief relative to the time scale of the K channels, then *W* does not have time to change much during the pulse, so, roughly speaking, only *V* is reset. The subsequent effect on *W* is seen in the post-stimulus response.

Figure 1.4a shows model voltage responses during and after a range of 2 ms stimulus pulses (amplitudes in Figure 1.4b). Before each pulse, the cell is at rest at $V = -60$. During the pulse, $I = I_{\text{stim}} > 0$ in Equation (1.12), and the voltage rises rapidly. Thus, at the end of the pulse, when *I* returns to zero, *V* has been "reset." After the pulse, the cell responds with classic threshold behavior: firing an action potential only if the reset *V* is sufficiently high.

In the next exercises, we will use XPP to explore the cell's post-stimulus response. Instead of modeling the stimulus pulse itself, we will reset the initial value of *V* directly – as a proxy for the cell's stimulus history – and plot *only* the post-stimulus response. In Section 1.4, we will see how

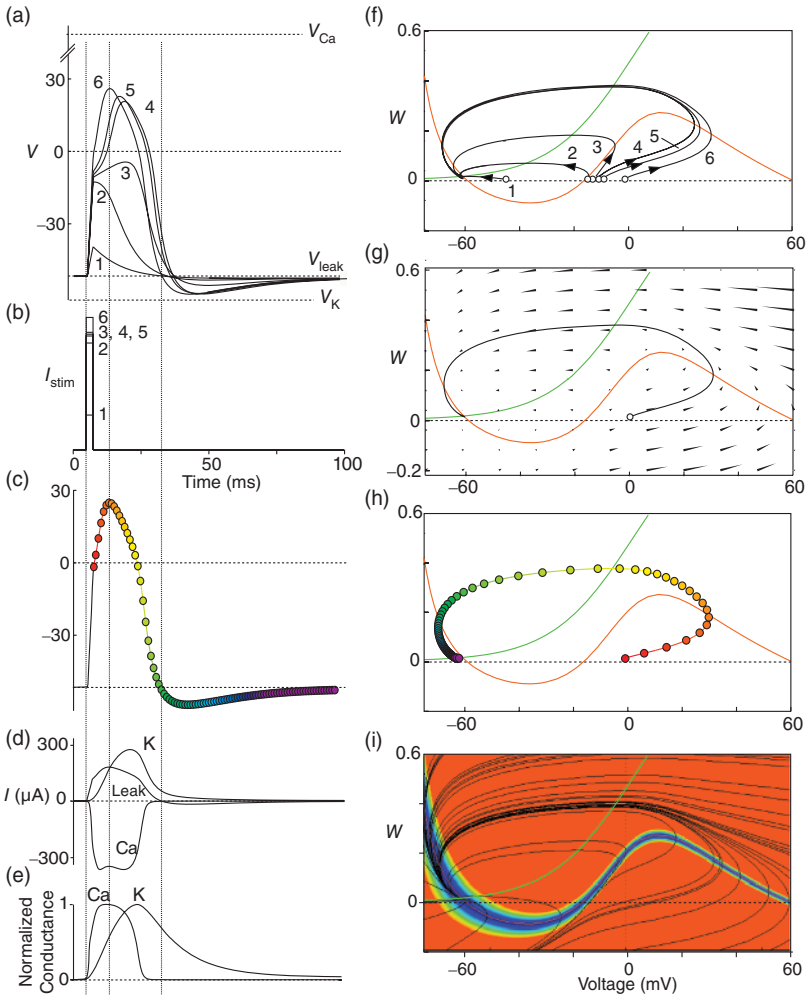

Figure 1.4 Model action potentials. Simulated response to a stimulus pulse, using Hopf parameter set. (a) Sub- and super-threshold voltage responses to the brief current steps in (b). Current amplitudes 1–6 were 150, 460, 480, 490, 500, and 570 μA, respectively. Responses 1 and 2 are below, 3 is near, and 4–6 are above firing threshold. (c) Voltages at 1 ms intervals for time course 6 in (a) (colored circles). (d) Model currents, and (e) normalized voltage-dependent conductances underlying response 6. Note the slower kinetics of K-current activation, despite similar *G*–*V* curves (Figure 1.3b), due to the different kinetic assumptions in the model. (f–i) Trajectories and nullclines (red and green, marking where *V* and *W* turn, respectively) in the phase plane. The intersection of the nullclines is a stable equilibrium; the ultimate destination of all trajectories after the brief stimulus pulse. (f) Trajectories corresponding to the voltage time courses in (a). An action potential corresponds to a counterclockwise excursion around the phase plane. (g) Trajectory 6 plotted with the direction field; vectors indicate the direction and rate of movement at any point in the phase plane. (h) Trajectory 6 plotted at 1 ms intervals, as in (c), indicating the speed of motion around the trajectory. The motion slows where V turns on the red nullcline, and where V approaches equilibrium. (i) The flow, represented by trajectories from many initial values in the phase plane. Color indicates speed of motion around the phase plane, from blue (slow) to orange (fast).

this approach lends itself to simultaneously plotting the cell's response to *all* possible histories on one graph, called the *phase plane*. (Note: if you wish to also explore the response during stimulus, an ODE file *BridgingTutorial-StimPulse.ode* is available on the website for this volume, or from the authors.)

(1.3.7) Continuing from Exercise 1.3.6, activate the XPP command window by clicking on it. Then click *(E)rase* to clear the graph. Click the *ICs* button, if necessary, to re-open the small window showing the initial conditions for V and W. Reset V to the depolarized value -30 (you may need to click once or twice in the box before you can erase or type in it). Leave W unchanged at 0, and click the *Go* button. How does the cell respond?

(1.3.8) The depolarization in the last exercise was evidently not strong enough to trigger an action potential, since the cell returned directly to rest. Try resetting the initial V to the more depolarized value -10, to represent a stronger stimulus. Now what happens?

(1.3.9) We saw in the last exercise that the cell fires an action potential if the stimulus is strong enough to reset V to -10 mV. Experiment with the initial V to see the decisive, all-or-nothing nature of the response, and reproduce the post stimulus responses of Figure 1.4a. Where is the firing threshold? In other words, approximately what is the smallest value of V that can trigger an action potential?

Dissecting the action potential. In the next exercises we will plot the post-stimulus time courses of the currents, conductances, and K-channel activation, W, that contribute to the action potential. Then, in Section 1.4, we will analyze the action potential from the phase-plane point of view, as in Figure 1.4f–i.

(1.3.10) To see the slow K-channel response, let us plot the post-stimulus time course of W. Click on the command window to activate it, then click on *(M)akewindow* in the menu, followed by *(C)reate* in the submenu. A new, small graphics window should open, showing a copy of the most recent V time course plotted. Notice that the new window does not have its own menu system. Instead, the command window menu applies to whichever graphics window is activated. A tiny black square in the upperleft corner of a graphics window indicates it is active. Activate the new window by clicking in it, and resize it to your taste. Click on *(V)iewaxes* in the menu, then *(2)D* in the submenu. Replace V with W for the *Y-axis*, and, since W is a proportion, set the Y range from a minimum of 0 to a maximum of 1. Note that you can also set the axis labels: t for the X label and W for the Y label. Then click the *OK* button. A W time course should appear in the new graphics window.

(1.3.11) The W time course you have plotted corresponds to the initial values of V and W currently displayed in the small *ICs* window (headed *Initial Data*). In case you have a confusion of too many plots at this point, you can clear each graphics window by activating it, and then clicking *(E)rase* in the menu. When both windows are clear, choose an initial condition just above firing threshold (e.g., $V = -13$), then click the *Go* button after activating each graphics window in turn.

(1.3.12) Resize and line up the W time course graphics window below the original V time course. Do you see how the K channels are slow, lagging behind the changes in V?

(1.3.13) You can also activate all the open graphics windows simultaneously. Click on *(M)ake window*, followed by *(S)imPlot On*. Click *(E)rase*, and notice that both the graphics windows are erased. (Recall that in Exercise 1.3.11 you had to erase one window at a time.) Now click the *Go* button, to see the V and W time courses plotted simultaneously in the two graphics windows. This can be very convenient, but it does slow XPP down, so remember to turn *(S)imPlot* off when you do not need it.

(1.3.14) In our ODE file *BridgingTutorial-MLecar.ode*, we define several *auxiliary quantities* (labeled *aux* in the ODE file), representing different components of the model response. Click on the *Equations* button at the top of the command window. A small window will pop up listing all the equations from the ODE file. You cannot edit the equations in this small window, but it is useful for reminding you of the names of the auxiliary quantities, and the roles of the parameters. Confirm that the auxiliary equations for the individual currents, conductances, and channel open probabilities agree with those developed in Section 1.2.

(1.3.15) Now click on the *Data* button at the top of the command window. A large window will pop up, in which the simulated data for each variable and auxiliary quantity are shown. This data can be exported to a space-delimited *dat* file using the *Write* button. Navigate around the data set using the *PgDn*, *PgUp*, *Right*, and *Left* buttons at the top of the window. Confirm that there are columns for all the auxiliary quantities. Also, confirm that the time increments are 0.25 ms and the total run time is 200 ms. Look back at the ODE file to see how these internal numerical parameters (*dt* and *total*) were pre-set, using the @ symbol.

(1.3.16) Each column in the data viewer can be plotted against time, or the columns can be plotted against each other. One way to plot a time course is by using *(V)iewaxes*, as in Exercise 1.3.10. A quick alternative is to click *(X)i* versus *t* in the menu, then enter the name of the variable or auxiliary quantitity to be plotted in the command line (using the name as it appears in the *Eqns* and *Data* windows). When you use *(X)i* versus *t*, the axes are automatically scaled to fit the data. The scale can then be adjusted using *(V)iewaxes*, if desired. Make three new graphics windows

(using *(M)akewindow*, then *(C)reate*). Line the new windows up underneath each other, and use *(X)i* versus t to plot the K conductance, the K driving force, and the K current (with initial V above firing threshold, at $V = -13$).

(1.3.17) Confirm that the graph of K conductance, given by $g_{Ca}W$, is the same shape as the graph of W, scaled by g_{Ca}.

(1.3.18) Why does the K driving force, given by $(V - V_K)$, start at 71 mV? Confirm that the graph of K driving force is an upward shift of the graph of V.

(1.3.19) The K current is given by $I_K = g_{Ca}W(V - V_K)$. Describe how the properties of the graph of the K-current result from the properties of the graphs of conductance and driving force. For example, why does the graph of I_K start at 0 μA? why does it peak at approximately 250 μA? and why does it drop more suddenly than the graph of K conductance?

(1.3.20) Let us plot the Ca conductance in the same window as the K conductance. Activate the window, then click on *(G)raphic stuff* in the menu, followed by *(A)dd curve* in the submenu, and enter CaCond for the *Y-axis* (the *Z-axis*, *Color*, and *Line type* can be ignored). Click Ok. Next, use *(V)iewaxes* to set the Y-axis range from 0 to 4 mS, so both graphs are visible. Confirm that, once again, the Ca channels lead the K channels. (In Figure 1.4e, we plot the normalized conductances, to help compare the kinetics.) Use the equation for Ca conductance in the *Equations window*, and the initial value of V, to explain the initial Ca conductance shown on your graph and in the data set.

(1.3.21) Next, plot the Ca driving force in the same window as the K driving force, using *(G)raphic stuff* and *(A)dd curve* again, after activating the appropriate window. At first, nothing new appears on the driving force graph. Explain why not. It might help to look at the data, or the value of V_{Ca}. Use *(V)iewaxes* to set the Y-minimum to −200 mV. Once again, the driving force is a vertical shift of the graph of V, but this time V is shifted down, representing an inward current.

(1.3.22) Now plot the Ca current on the same graph as the K current, and confirm that it is an inward current, adjusting the axis range as needed (see Figure 1.4d). As before, describe how the properties of the graph of the Ca current result from properties of the graphs of conductance and driving force.

In *silico experiments with XPP.* We hope that you are inspired to experiment independently. You could plot the currents and conductances for an initial V just *below* firing threshold; you could adapt the building blocks developed in the Morris–Lecar model to include more channels or more complex gating properties (see Chapter 2 for inspiration); or you could include calcium dynamics (see Chapters 3 and 4 for inspiration). You could then compare

model behaviors to clarify the roles of different channels, gating nuances, and your model assumptions.

Hodgkin–Huxley and Fitzhugh–Nagumo models. The XPP download comes with ODE files for several models of excitability. The Hodgkin–Huxley model (Hodgkin and Huxley, 1952), includes both activation and inactivation, and the kinetics are more realistic, reflecting the number of gating domains required to be in the corresponding state. In the Fitzhugh–Nagumo model (Fitzhugh, 1961; Nagumo *et al.*, 1962), the terms have been abstracted to capture, as simply as possible, the essential geometric features of the nullclines (defined in the next section) that underlie excitability. These and other models recur throughout the text, illustrating the art of letting the biological question determine the level of model complexity to use. They are discussed in most texts on theoretical neuroscience, such as Edelstein-Keshet (2005), Ermentrout and Terman (2010), Fall *et al.* (2005), Izhikevich (2007), Keener and Sneyd (2008), or Koch (1999).

1.4 Action potentials in the phase plane

In this section, we take a different view of the action potential. We exploit the fact that the Morris–Lecar model has only two dependent variables (V and W) to plot them against each other instead of plotting each against time. Then we see how graphical analysis of the resulting *phase plane* yields surprisingly many insights into the behavior of the model, through an appeal to our geometric intuition.

(1.4.1) Let us start afresh. If XPP is not already open, then fire it up with *BridgingTutorial-MLecar.ode*. If you still have XPP open with lots of graphics windows from the last section, then clean up by clicking *(M)akewindow*, then *(K)ill all* (a tiny pop-up window will ask if you are sure). If you have been experimenting with different values for the parameters, then click on *(F)ile*, followed by *(G)et par set* and select *hopf* to restore the default parameters of the Hopf column of Table 1.1. (Look back at the ODE file to see how the parameter set choices available in *(F)ile*, *(G)et par set* are coded using the *set* command.) Set the initial V and W to -13 and 0, respectively. Plot an action potential in the graphics window, and open the data viewer (*Data* button in the command window).

Trajectories in the phase plane. The first three columns of simulated data are time, voltage (V), and K-channel activation (W). The familiar voltage trace (or time course) is graphed by plotting the time and voltage columns against each other, but there are many other ways of visualizing the same data.

A *trajectory* in the *phase plane* is graphed by plotting the V and W columns against each other.

(1.4.2) Let us plot the trajectory corresponding to the action potential in Exercise 1.4.1. Make a new window (*(M)akewindow, (C)reate*), and use *(V)iewaxes, (2)D* to choose V for the x-axis and W for the y-axis, setting the *Xlabel* and *Ylabel* accordingly. Set V to range from -80 to 60, and W to range from -0.2 to 0.6. (Note that channel activation cannot, in reality, be negative. Our reason for including the negative range is to make it easier to see what's going on when $W = 0$).

(1.4.3) At first glance the trajectory does not look much like an action potential. We will examine it more closely, to recognize the familiar components of excitability embedded within it. The first row in the data viewer corresponds to time 0 ms, so $V = -13$ mV and $W = 0$ (the initial conditions we chose in Exercise 1.4.1). Locate the corresponding point $(V, W) = (-13, 0)$ in the phase plane. This is where the trajectory starts.

(1.4.4) Each subsequent row in the data viewer represents a small step forward in time, and each corresponding (V, W) point is plotted in the phase plane. The resulting curve is the *trajectory with initial condition* $(V, W) = (-13, 0)$. Use the *Down* button at the top of the data window to confirm that when $t = 10$ ms, V is approximately 8.3 mV and W is approximately 0.13. Locate the corresponding point on the trajectory.

(1.4.5) As time progresses, the cell continues around the trajectory. What is the peak voltage reached? When does it peak? What proportion of K channels are open when it peaks? Which of these questions can be answered using: (i) the phase plane? (ii) the voltage trace? (iii) the data viewer? Confirm that they give the same answers, where applicable.

Translating between a time course and the phase plane. It takes some practice to relate the "vertical" voltage axis of the time course to the "horizontal" voltage axis of the phase plane. Figure 1.4c and h illustrates how motion around the phase-plane trajectory corresponds to the action potential time course. The dots mark equal time intervals of 1 ms. There is no time axis in the phase plane. Instead, the progression of time is captured by progression around the trajectory. (The solid red and green curves in the phase plane are the *nullclines*, defined later in this section.) During the rapid depolarization and hyperpolarization segments of the spike in the voltage trace, voltage (V) is changing much faster than K-channel activation (W), thus yielding the rapid, roughly "horizontal" segments of the trajectory in the phase plane. Around the peak of the voltage trace, and during hyperpolarization, the voltage changes more slowly, so the K channels have time to open (close, respectively), and the motion around the phase plane has more "vertical" component. As voltage gradually returns to rest, W also stabilizes,

and the trajectory approaches an *equilibrium point* in the phase plane. In summary, the explosive action potential characteristic of excitability corresponds to a large counterclockwise excursion around the phase plane before returning to equilibrium.

(1.4.6) Figure 1.4f shows six trajectories in the same phase plane, corresponding to the post-stimulus components of the six voltage traces in Figure 1.4a. Each trajectory has a different initial condition, as set by the pulsatile stimuli shown in Figure 1.4b. Which of the trajectories has initial condition $(V, W) \approx (-13, 0)$? And which has the initial condition $(V, W) \approx (-14, 0)$? Explain how you know.

(1.4.7) More generally, any point (V, W) in the phase plane can be used as initial data for the model. XPP allows you to select initial points with the mouse as follows. Activate the phase plane, then click *(I)nitialconds* in the side menu of the command window (not the *ICs* window we have used so far.) Select *m(I)ce* in the submenu. A tiny pop-up window appears with instructions. Experiment with initial points all over the phase plane. Press the *escape* key to exit this mode of choosing initial points when you are ready. Recall that we can view the initial condition of our model cell as reflecting its recent history. What history could lead to each initial point you chose? Some of them are more physiologically meaningful than others. Do the corresponding trajectories make sense? Remember you can turn *(S)implot* on (in the *(M)akewindow* menu), if you would like to see the corresponding voltage traces simultaneously, and you can click *(E)rase*, for a fresh start.

(1.4.8) The family of all trajectories is called the *flow* of the system. Erase everything, and turn *Simplot* off (it is off if the menu toggle offers to turn it on). To plot a representative sample of the flow, called a *phase portrait*, activate the phase plane and click on *(D)ir. field/flow*, followed by *(F)low*. Press *return* to accept the suggestion, in the command line, of a 10×10 grid of initial points, and watch the beautifully flowing dynamics emerge. Try experimenting with different sized grids.

The phase portrait shows the full range of behavior. A powerful feature of the phase plane is that it shows the cell's response to all possible histories, all at once. It gives immediate intuition for the full range of responses this cell can exhibit. The cell can fire at most one action potential and all trajectories eventually settle at the same rest point. The "all-or-nothing" quality of the response is captured by the very thin threshold region dividing trajectories that take the large, counterclockwise excursion from those that return directly to rest, and we see that there is, in fact, some variability in the amplitude of the excursion (or spike). In later sections, we will explore how a sustained stimulus expands this range of behaviors.

Trajectories never cross. Another powerful feature of the phase plane is that trajectories may flow toward each other, but they never cross. This has profound consequences for two-dimensional systems, because it means each trajectory imposes a spatial barrier to all the others, trapping them in different regions of the phase plane. This fundamental geometric fact that one-dimensional curves form barriers in a two-dimensional plane explains why geometric phase-plane analysis is so powerful, and can lead to qualitative predictions with relative ease. To understand why trajectories cannot cross each other, it is helpful to relate our model equations (1.12)–(1.16) directly to the phase plane:

(1.4.9) Equations (1.12) and (1.13) govern the time course of V and W for our model cell. Using $(V, W) = (-13, 0)$, and the parameter values in the Hopf column of Table 1.1, do the calculations to confirm that $M_\infty(V) \approx 0.21$, $W_\infty(V) \approx 0.27$ and $\tau_W(V) \approx 0.97$. Thus, the rate of change of V is $\frac{dV}{dt} \approx 0.95$ mV/ms, and the rate of change of W is $\frac{dW}{dt} \approx 0.01$ ms^{-1}.

(1.4.10) At the rates given in Exercise 1.4.9, in 1 ms, V would increase by 0.95 mV to -12.05 mV and W would increase from 0 to 0.01. Carefully sketch, on paper, the arrow, or *vector*, pointing from the initial point $(V, W) = (-13, 0)$ to the new point $(V, W) = (-12.05, 0.01)$. Your vector has components $\left(\frac{dV}{dt}, \frac{dW}{dt}\right) = (0.95, 0.01)$, and shows the instantaneous direction of motion that a trajectory passing through the point $(V, W) = (-13, 0)$ *must* follow. Use XPP to plot the trajectory with initial condition $(-13, 0)$, and confirm your direction vector agrees with the direction of the trajectory at $(-13, 0)$. (You may need to adjust the scale on the axes to make the comparison.)

(1.4.11) The *direction field* of the system consists of the vectors $\left(\frac{dV}{dt}, \frac{dW}{dt}\right)$ representing the direction of motion all over the phase plane. To plot a representative sample of direction vectors, as shown in Figure 1.4g, activate the phase plane and click on *(D)ir. field/flow*, followed by *(D)irect Field*, and press *return* to accept a 10×10 grid of initial points.

(1.4.12) Revisit Exercises 1.4.9 and 1.4.10 to confirm that the different lengths of the direction vectors indicate the relative speed of motion around the phase plane. (In contrast, *(D)ir. field/flow*, followed by *(S)caled Dir. Fld*, shows all the direction vectors scaled to the same length.)

(1.4.13) Choose initial conditions (using *(I)nitialconds, m(I)ce*) to superimpose individual trajectories on the direction field (as shown in Figure 1.4g). Alternatively, you can superimpose the flow (as demonstrated in Exercise 1.4.8). Notice that trajectories always travel in the direction of motion dictated by the direction field. This is not a coincidence. This is what it means for trajectories to be *solutions* of the system of differential equations (1.12) and (1.13). Now, it is clear why trajectories cannot cross each other. They have to follow the direction field. And the direction field cannot point in two different directions at once.

Autonomous systems. This is a good moment to emphasize that the argument we just used, and the entire phase-plane viewpoint, depends on the fact that our model equations (1.12)–(1.16) are *autonomous*. Recall from Section 1.2 that this means that the independent variable, time, does not appear explicitly on the right-hand side of the equations. So the direction vector through a given point (V, W) does not change over time, and can only point in one direction.

Nullclines. Recapping, we have seen that the range of behaviors our model cell can exhibit is predicted by the flow in the phase plane. The flow, in turn, follows the direction field, which is given by the differential equations. We now introduce the *nullclines* of the system, which give a quick guide to how the direction field is organized.

(1.4.14) Erase everything and plot the flow with a 10×10 grid (*e, d, f,* then *return*, via shortcut keys). Now plot the nullclines by clicking on *(N)ullcline*, and then *(N)ew*. (Recall that you can hover over each menu item for a description along the bottom of the command window, if you wish). There are two nullclines, one red and one green, as in Figure 1.4f–i. How can you tell the nullclines are *not* trajectories? (Hint: trajectories do not cross.)

(1.4.15) So what are the nullclines? Let us uncover their meaning from the XPP plot, starting with the red nullcline. What do you notice about the direction of the trajectories as they cross the red nullcline? And what would that correspond to on the associated voltage traces? It may help to make your graphics window huge, and redraw everything.

Nullclines mark turning points. The trajectories always "turn back" on themselves at the red nullcline. Below the red nullcline, trajectories flow to the right (as well as flowing "up" or "down" the phase plane). At the nullcline they turn, so that above the red nullcline trajectories flow to the left. Those that reach the red nullcline again, at the far left of the graph, turn again, flowing gently rightwards towards the equilibrium point. This observation yields the definition. Rightward and leftward flow in phase space correspond to increase and decrease in voltage, respectively. Thus, the red nullcline marks the points in the phase plane where the voltage turns. In more biological words it marks the peaks and troughs of the corresponding voltage trace. In more mathematical words, it marks the points where the graph of V against t has a maximum or minimum (or inflection point). So the red nullcline marks the points where $\frac{dV}{dt} = 0$, and is, therefore, called the *V-nullcline*.

(1.4.16) Recall from Exercises 1.4.9 to 1.4.11 that the direction field consists of the vectors $\left(\frac{dV}{dt}, \frac{dW}{dt}\right)$ evaluated at each point. Use this to explain

as to why the flow is parallel to the W axis as it crosses the V-nullcline. (Hint: $\frac{dV}{dt} = 0$ on the *V-nullcline*.)

(1.4.17) The (green) W-nullcline is defined analogously. Use your XPP plot to confirm that $\frac{dW}{dt} = 0$ on the green nullcline. In other words, flow across the W-nullcline is parallel to the V axis, and the nullcline marks the points where trajectories turn from increasing W (K channels opening) to decreasing W (K channels closing), or vice versa.

Nullclines organize the direction field. Presently, we will examine how the shape of the nullclines is derived from the model equations. First, we will explore how the nullclines mark equilibria and organize the direction field, giving a rough, but immediate, guide to the dynamics of the system.

(1.4.18) Erase everything, and plot the direction field with a 10×10 grid (*e, d, d* then *return*). If the nullclines do not redraw automatically, plot them again (*n, n*). The nullclines divide the phase plane into regions. Confirm that, in each region, the direction vectors all point in roughly the same direction or *quadrant* (e.g. upward and rightward, or upward and leftward, etc.) Explain why. (Hint: nullclines mark turning points).

(1.4.19) What happens at the point where the two nullclines meet? Let us call it point P. Try choosing initial conditions exactly at P (using *i,i*). Nothing appears to happen. Why? (Remember to *escape* from *i,i* mode when you are done.)

Equilibria lie at the intersection of nullclines. The point P lies on both nullclines, so both $\frac{dV}{dt} = 0$ and $\frac{dW}{dt} = 0$ at P. Thus, from initial point P, there is no change in V or W, the direction vector reduces to $(0, 0)$, and the trajectory is fixed at P for all time. We call P an *equilibrium* or *fixed point* of the system. By the same argument, every intersection of the two nullclines yields an equilibrium, and every equilibrium lies at an intersection of the nullclines.

(1.4.20) Try choosing initial conditions close to P (using *i,i* again). Confirm that trajectories from all nearby initial conditions converge to P. In other words, P represents rest, where our model cell stabilizes. Thus, we call P a *stable* equilibrium or *attractor*.

Stable versus unstable equilibria. We classify the stability of an equilibrium according to the behavior of the system *near* the equilibrium. If nearby initial conditions are all attracted to an equilibrium, it is *stable*. If they are generally repelled from the equilibrium, it is *unstable*. The very fact that systems settle down at stable equilibria makes them easy to observe in nature and experimentally, while unstable equilibria are much more

difficult to observe. In the next sections, we will see how stable and unstable phenomena interact to shape both the transient and long-term dynamics of the system.

What determines the shape of the nullclines? We will use a combination of algebra and XPP experiments to develop intuition for the nullcline shape. Algebraically, each nullcline can be viewed as the graph of some equation of the form $W = f(V)$ in the V–W phase plane. We will find these equations, to see which model parameters influence each nullcline.

W-nullcline. We will start with the W nullcline, because the algebra is simpler. Recall that the W component of direction vectors in the phase plane is given by Equation (1.13)

$$\frac{dW}{dt} = \frac{\phi}{\tau_W(V)}(W_\infty(V) - W)$$

Also, recall that the W-nullcline marks the points where $\frac{dW}{dt} = 0$. Thus, points on the W-nullcline satisfy the equation

$$0 = \frac{\phi}{\tau_W(V)}(W_\infty(V) - W) \tag{1.17}$$

From our model assumptions, we know the time scale $\frac{\phi}{\tau_W(V)}$ is positive and non-zero. So Equation (1.17) can be simplified and rearranged to yield the desired equation for the W-nullcline

$$W = W_\infty(V) \tag{1.18}$$

In other words, the green, W-nullcline is the familiar graph of steady-state K-channel activation $W_\infty(V)$ given by Equation (1.15), shown in Figures 1.3b and c, and explored in Exercises 1.2.4–1.2.7. Thus, points on the W-nullcline satisfy the equation

$$W = 0.5\left(1 + \tanh\left(\frac{V - V_3}{V_4}\right)\right) \tag{1.19}$$

In retrospect, this makes sense: we developed the K-channel kinetic model so that K-channel activation, W, is always playing catch-up to the voltage-dependent, "steady" state, $W_\infty(V)$. If, at a point (V, W) in the phase plane, W is lower than the corresponding $W_\infty(V)$, then W will increase to catch up. In other words, below the graph of $W_\infty(V)$, W increases. Above the graph of $W_\infty(V)$, W decreases. Thus, the graph of $W_\infty(V)$ is the W-nullcline, marking the points in the phase plane where W turns in its quest to follow the elusive $W_\infty(V)$.

(1.4.21) Using *(V)iewaxes, (2)D*, expand the V axis to range from −100 mV to 100 mV, and the W axis to range from −0.2 to 1.2. Erase everything (*e*), and redraw the nullclines (*n,n*) to confirm that the green, W-nullcline is, indeed, the graph of $W_\infty(V)$.

(1.4.22) Click on *Par/Var* in one of the slider bars at the bottom of the command window to set up a slider, ranging from −50 to 50 mV for the half-activation (V_3) of steady-state K-channel activation. (Note that *SimPlot* slows down the slider bars considerably, so it is helpful to turn if off (in the *Makewindow* menu) if not needed.) What happens to the W-nullcline as you slide V_3? Explain why.

(1.4.23) Shift the W-nullcline to the right, so that it crosses the V-nullcline again and there are three equilibria. Plot trajectories starting close to each of the equilibria (*i,i*) to determine whether each equilibrium is stable or unstable. Confirm that the stability of the rightmost equilibrium depends on how much V_3 has been shifted. Also, plot the flow (*d, f* then *return*) to see how the local behavior, close to the equilibria, is globally connected. Describe the overall behavior of the model cell. It may help to plot the voltage traces for some trajectories. Does the change in behavior as V_3 increases make physiological sense?

(1.4.24) Set up another slider for the spread (V_4) of steady-state K-channel activation, ranging from 10 to 50 mV. Confirm that, for intermediate values of V_3, changing V_4 can also change the number of equilibria and overall behavior of the system.

V-nullcline. It takes more work to develop intuition for the "folded" (or roughly "cubic") shape of V-nullcline, because more of the parameters play a role in the associated differential equation. Nevertheless, we can follow the same approach we used for the W-nullcline. Recall that the V component of direction vectors is given by Equation (1.12)

$$C\frac{dV}{dt} = I - g_{\mathrm{Ca}}M_\infty(V - V_{\mathrm{Ca}}) - g_K W(V - V_K) - g_{\mathrm{L}}(V - V_{\mathrm{L}})$$

The V-nullcline marks the points where $\frac{dV}{dt} = 0$. Thus, points on the V-nullcline satisfy

$$0 = I - g_{\mathrm{Ca}}M_\infty(V - V_{\mathrm{Ca}}) - g_{\mathrm{K}}W(V - V_{\mathrm{K}}) - g_{\mathrm{L}}(V - V_{\mathrm{L}}) \tag{1.20}$$

Bringing the K-current term to the left-hand side, we have

$$g_{\mathrm{K}}W(V - V_{\mathrm{K}}) = I - g_{\mathrm{Ca}}M_\infty(V - V_{\mathrm{Ca}}) - g_{\mathrm{L}}(V - V_{\mathrm{L}}) \tag{1.21}$$

Then, rearranging to isolate W on the left-hand side yields the equation for the V-nullcline in the V–W plane

$$W = \frac{I - g_{\mathrm{Ca}}M_\infty(V - V_{\mathrm{Ca}}) - g_{\mathrm{L}}(V - V_{\mathrm{L}})}{g_{\mathrm{K}}(V - V_{\mathrm{K}})} \tag{1.22}$$

(1.4.25) Reset your initial condition close to threshold, and experiment with different values of the model parameters appearing in Equation (1.22), including those hidden in Equation (1.14) for M_∞, to see their role and effect on the V-nullcline, equilibria, direction field, flow and voltage traces. Parameter values can be changed using the parameter window (click on the *param* button at the top of the command window, then enlarge the window to see all the parameters), or by using the slider bars. You can reset the parameters to their default values using *(F)ile, (G)et par set* then *hopf*. As you experiment, pay particular attention to:

- The way the shape and position of the nullclines dictate the number of equilibria (intersections). The number of equilibria is typically 1 or 3. Why is it so rare to have exactly two equilibria?
- The way the nullclines and direction field change together, so that trajectories always turn at the nullclines, and in each region defined by the nullclines, direction vectors point into the same quadrant.
- Changes to the firing threshold and overall behavior. Do they make physiological sense for your parameter changes?

Summarizing. With the help of XPP, we have seen how the Morris–Lecar model, with its minimal mechanism of one excitatory and one depolarizing current, qualitatively reproduces some basic characteristics of excitable cells; firing an action potential when the stimulus is sufficient to cross firing threshold. We can plot the voltage trace and the currents contributing to the action potential, and translate between these traditional time courses and the phase plane; an action potential in the voltage trace corresponds to an excursion around the phase plane, and resting potential corresponds to an equilibrium. We can also use these plots in concert to gain a fuller understanding of the model cell's behavior. The time courses show the detailed response to a single stimulus history or initial condition, while the phase plane shows the qualitative response to all initial conditions at once. Within the phase plane, the direction field indicates how the flow is generated from the differential equations, and the nullclines are useful for locating the equilibria and showing how the flow is organized.

Many of these ideas generalize to the concept of *phase space* for autonomous systems in higher dimensions, which is useful as we add more variables to our models. As the number of variables increases, the geometry gets harder to visualize, so we have to introduce more mathematical formalism to describe the model dynamics. The geometric nature of the phase plane makes it an excellent point of contact, where experimentalists and theoreticians can learn enough about each others'

language to spark collaborations about more complex biological systems modeled in higher dimensions.

For more about the phase plane and its generalizations, see any introductory text on dynamical systems, such as Blanchard *et al*. (2011), Hirsch *et al*. (2012), or Strogatz (1994).

1.5 Model response to sustained current injection

In the next few sections, we take a tour through parameter space, following the route mapped out by Rinzel and Ermentrout (1989), to explore the surprising richness of behavior the Morris–Lecar model cell exhibits in response to a simulated current clamp experiment in which sustained current is applied to a cell at rest.

Recall that in Sections 1.3 and 1.4, we discussed a current clamp experiment in which a brief stimulus current was applied to set the cell's initial condition. The applied current, I, was then returned to zero, and the cell's post-stimulus response was analyzed in the phaseplane corresponding to $I = 0$. Henceforth, the simulated current clamp experiments are different, in that the applied current is sustained indefinitely. Each different current amplitude corresponds to a different phaseplane, and the model behavior changes accordingly.

Most of the time the behavior changes gradually as I changes. But occasionally a small change in applied current leads to a qualitatively dramatic change in behavior. Mathematically, these qualitative changes arise through *bifurcations*, which are most easily understood in the phaseplane. Different bifurcation mechanisms correspond to different characteristics of excitability, and our tour through parameter space will introduce us to the bifurcations that occur most commonly in two-dimensional systems. We continue, in this section, with the parameter set "Hopf" from Table 1.1.

(1.5.1) From now on, it will be convenient to have the phaseplane as the default graph in the command window, and to open a secondary voltage trace window. So quit XPP (*(F)ile,(Q)uit,(Y)es*), and look back at the ODE file (*BridgingTutorial-MLecar.ode*) to see how the default axes and their ranges were set, using the @ symbol. Edit the ODE file to comment out the line that sets the x- and y-axes as t and V, respectively, and uncomment the line that sets the x-axis as V and the y-axis as W. Also, in the line headed *some numerical settings*, reset the *total* (run time) from 200 to 500.

(1.5.2) Re-open XPP. Now the command window should show the phase plane, with V ranging from −75 to 70 mV on the x-axis, and W ranging from −0.2 to 1 on the y-axis. Open a second window for the voltage trace using *(M)akewindow, (C)reate* then set t from 0 to 500 ms on the x-axis, and V from −80 to 60 mV on the y-axis using *(V)iewaxes, (2)d*.

Open the parameter window (using the *param* button at the top of the XPP window) and check that the parameters agree with the Hopf column of Table 1.1. If not, select the Hopf parameter set using *(F)ile, (G)et par set*.

(1.5.3) Let us explore the impact of sustained current on the voltage trace first, then we will take the phase-plane view. Set up a slider for I ranging from 0 to 275 using one of the slider bars at the bottom of the command window. Activate the voltage trace window by clicking on it (recall that a tiny black dot in the top left corner of a graphics window tells you which window is active), then use the slider to gradually increase I. Notice the sudden changes in the voltage trace, and compare your simulations with Figure 1.5. The cell starts at rest. Small values of the applied current increase the resting potential. Around $I = 73$, a single action potential is triggered. As you continue to increase I, the applied current pushes the "resting potential" across firing threshold so that there is a sudden onset of repetitive spiking just before $I = 96$. The spiking behavior continues as I is increased, until it suddenly disappears around $I = 239$, and the voltage settles to a plateau level.

(1.5.4) Now let us take the phase-plane viewpoint. Return the slider to $I = 0$, activate the phase-plane window and plot the nullclines (*(N)ullcline, (N)ew*). Gradually increase I, and notice how changes in the trajectory in the phase plane correspond to changes in the voltage trace, as in Figure 1.5. What phase-plane behavior corresponds to tonic spiking? (Note, if you turn simplot on (*(M)ake window, (S)implot on*), then the slider applies to both graphs at once, but operates more slowly. Alternatively, you can keep simplot off, and switch between graphs by activating the window you want, erasing the old graph (*e*), restoring a plot of the most recent simulation (*r*), and replotting the nullclines if in the phaseplane (*n,n*)).

Tonic spiking corresponds to a limit cycle. The sudden appearance of tonic spiking in the voltage trace corresponds to the appearance of a *limit cycle* (or closed loop, or *periodic orbit*) in the phaseplane. The trajectory no longer settles at an equilibrium (or rest point), but instead travels endlessly round and round the limit cycle, tracing out repeated action potentials. In the next exercises, we will consider the role of the nullclines and equilibrium in shaping the voltage waveform.

(1.5.5) What happens to the each of the nullclines as you increase I? Look back at the role of I in the nullcline equations (1.19) and (1.22) to explain why the (red) V-nullcline moves upwards, while the (green) W-nullcline stays fixed. Recall that the equilibrium is at the intersection of the two nullclines. Slide I up and down again, and watch how the equilibrium gradually travels up and down the W-nullcline at the same time as it

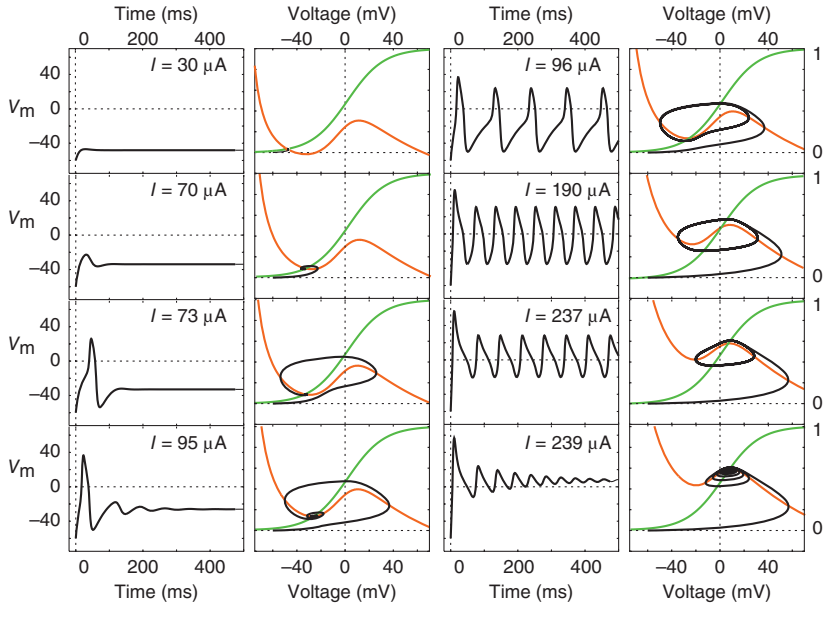

Figure 1.5 Sustained current injection with the Hopf parameter set. Model responses to a progressive series of sustained current stimuli (amplitudes indicated), showing voltage traces in time and the corresponding phase-plane trajectories and nullclines. As stimulus amplitude begins to increase, single action potentials are elicited. At a sharply defined value close to $I = 96$ μA, repetitive trains of action potentials are elicited, corresponding to the sudden appearance of a stable limit cycle in the phase plane. At this point, the firing frequency is immediately at a characteristic non-zero value (determined by the speed around the cycle), from which it increases only modestly over a wide range of stimulus currents, as in Hodgkin's Class II neurons. At another sharply defined stimulus amplitude, just below $I = 239$ μA, the stable cycle and corresponding spike train are suddenly lost, and voltage damps to a stable equilibrium at relatively positive potential.

travels back and forth along the V-nullcline. Pay close attention to the cycling behavior of the trajectory as the equilibrium travels past the local maximum and minimum (turning points) of the V-nullcline. Do you see a pattern? Roughly speaking, when the equilibrium is on the middle branch of the V-nullcline, between the turning points, there is tonic spiking. When the equilibrium is outside the middle branch the voltage settles down to the equilibrium value.

(1.5.6) For another insight into the role of the nullclines, plot the scaled direction field (*(D)ir. field/flow, (S)caled Dir.Fld*). Click the *return* key to accept the default 10×10 direction field grid suggested in the XPP command line. Recall, the arrows show the direction of motion of a trajectory as it travels around the phase plane. On the W-nullcline, there is no motion in the W direction, so arrows with "feet" on the W-nullcline

are perfectly horizontal (the dots represent the arrowheads). Similarly, arrows with feet on the V-nullcline are perfectly vertical. Use these facts to explain why the left and right extremes of a limit cycle lie on the V-nullcline. What do these extremes correspond to on the voltage trace? Now, slide I up and down, and watch how the arrows change direction as the V-nullcline passes by. How do these geometric observations relate to the balance of currents in the cell?

(1.5.7) It can also be instructive to repeat Exercise 1.5.6 on a finer scale to examine the sudden appearance of the limit cycle. Recall that the cycle appears around $I = 96$. Set $I = 90$, and temporarily reduce the slider range of I from 90 to 100. Nudge the slider to update the phase-plane image, then zoom in to a smaller box around the trajectory. (Click *(W)indow/zoom*, then *(Z)oom In*, and use the cursor to select the region of interest). The nullclines might not look smooth after zooming in. You can fix that by erasing everything (*e*), and redrawing the nullclines and scaled direction field, but it will also fix itself when you move the I slider. Slide I up and down. How does the subtle geometric interaction of the nullclines and direction field contribute to the sudden appearance of the limit cycle? You may find it helpful to redraw the scaled vector field on a finer, 30×30, grid.

Stability of the equilibrium versus the limit cycle. Recall that the stability of an equilibrium is about the behavior of the system near the equilibrium. If nearby initial conditions are attracted to the equilibrium, it is stable. If they are generally repelled from the equilibrium, it is unstable. The same concept of stability applies to the limit cycle: if nearby initial conditions are attracted to the cycle, it is stable; if they are repelled, it is unstable.

(1.5.8) For a clean start, erase everything (*e*), return the phase-plane window to default scale (*(W)indow/zoom, (D)efault*), and reset the I slider from 0 to 250. Choose a value of I, plot the nullclines (*n,n*) and test the stability of the equilibrium by checking what happens to nearby initial conditions. An easy way to do this is to choose *(I)nitital conditions* then *m(I)ce*. After clicking to activate the phase-plane window, you can choose lots of initial conditions with the mouse. When you are done, nudge the slider, or click *escape*, to liberate your mouse. Try it for a range of values of I to explore the stability of the equilibrium as it travels along the nullclines and the limit cycle appears and disappears. Is the equilibrium stable or unstable when there is a limit cycle? How about when there is no cycle? The case of a single action potential is like in Section 1.4. The equilibrium is stable, even tho some initial conditions take a large excursion before returning to rest.

(1.5.9) When there is a limit cycle, is it stable or unstable?

Exchange of stability. Roughly speaking, the equilibrium appears to be stable when there is no limit cycle, but unstable when there is a limit cycle. The limit cycle itself is stable, as if the equilibrium had passed its stability to the cycle. In fact, if you test initial conditions closely, right around the appearance and disappearance of the limit cycle, you will see the situation is a bit more subtle. We will return to that subtlety with the bifurcation diagram in Section 1.6.

The influence of instability. Unstable behavior is, by nature, very difficult to observe experimentally. For example, we have just seen that when the equilibrium is unstable in our simulations we observe tonic spiking instead. We might be tempted to argue that unstable behavior is irrelevant to biology. But invisible, unstable phenomena can play important roles in shaping the observable, stable behavior of a system. We will develop intuition for this fact in the next two exercises by exploring how the unstable equilibrium influences the voltage waveform when the cell is spiking.

(1.5.10) Reset the initial condition to $(V, W) = (-60, 0)$ (by clicking on it, or in the ICs window), and turn on the (unscaled) direction field (*(D)ir. field/flow, (D)irect field, return*). Recall that in the unscaled direction field, the length of the direction vector indicates the relative speed of motion around the phaseplane. Slide I up and down, and confirm that the arrows are very short near the equilibrium. Why is that? Use the definition of an equilibrium to explain. If you are not convinced, try zooming in closer to the equilibrium, or increasing the number of grid points.

(1.5.11) Set $I = 96$. Where is the equilibrium relative to the limit cycle? Activate the voltage trace window, and graph the waveform (*i,g*). Which part of the waveform corresponds to the stretch of the limit cycle closest to the equilibrium? For example, is it the depolarizing or hyperpolarizing phase of the action potential? Is it close to the peak or minimum voltage? The direction arrows are shortest close to the equilibrium, so the motion is slow. How is that reflected in the voltage waveform? Now, gradually increase I, so that the unstable equilibrium moves towards the middle of the limit cycle. What impact does this have on the voltage waveform and why does the spike frequency increase? Finally, increase I to a value just before the limit cycle disappears. Why does the spike frequency decrease again? And why does the waveform develop the "shoulders" seen in some cells?

Summarizing. As we increase I in this simulated current clamp experiment, there are two areas of qualitatively dramatic change: the onset and offset of tonic spiking, corresponding to the appearance and disappearance of a limit cycle in the phaseplane. There is an associated exchange of stability between the equilibrium and the limit cycle, but, even while unstable, the

equilibrium continues to influence the waveform of the spikes. In the next section, we examine the *bifurcations* underlying the qualitative changes in behavior, and learn how to read the associated *bifurcation diagram*.

1.6 Reading a bifurcation diagram

We hope that the previous section convinced you that there is a value in studying both the stable and unstable behavior in a model. Sherman (2011) gives a nice analogy: the system is like a Shakespeare play, where some of the action is on-stage and observable, but influential events also happen off-stage, to be perceived only indirectly by their on-stage impact. Figure 1.6 shows the *bifurcation diagram* for our simulated current clamp experiment, succinctly summarizing information about all the stable and unstable equilibria and limit cycles. There is a lot of information packed into a bifurcation diagram, so we will spend some time unpacking it in this section. The *bifurcation parameter*, on the x-axis, is the parameter being controlled (applied current, in our case). The variable of interest (voltage) is plotted on the y-axis.

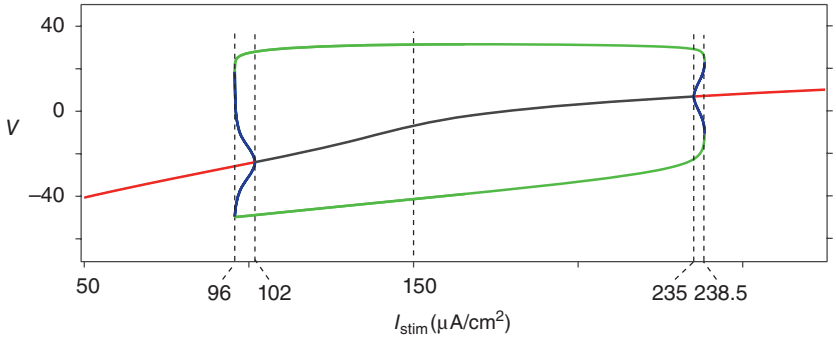

Figure 1.6 Bifurcation diagram for the Hopf parameter set. The diagram summarizes the behavior illustrated in Figure 1.5. Stimulus current, I, is the bifurcation parameter, and voltage, V, is the behavior variable plotted. For each value of the stimulus current, there is a corresponding phase plane, as shown in Figure 1.5. The equilibria and limit cycles from all the phase planes are charted on the bifurcation diagram, to show how they vary with stimulus current, and to highlight the bifurcations. The equilibrium voltage in each phase plane is plotted on the bifurcation diagram against the corresponding stimulus current; in red if the equilibrium is stable and in black if it is unstable. A limit cycle is represented by its peak and trough voltage levels; in green if the cycle is stable and in blue if it is unstable. In the simulated experiment in Section 1.5, repetitive firing begins where the branch of unstable limit cycles, born at the subcritical Hopf bifurcation ($I = 102$ μA), appears to fold back on itself to become stable, at the saddle-node bifurcation of limit cycles ($I = 96$ μA). Firing terminates in a similar mechanism. Note the regions of bistability around the onset and offset of spiking, where a stable equilibrium and stable limit cycle coexist.

(1.6.1) Locate the value $I = 150$ on the X-axis in Figure 1.6. There are three points on the bifurcation diagram at this value of I. What is the (approximate) value of the voltage at the black (middle) point? Use XPP to confirm that it is the voltage of the equilibrium (in the phaseplane) when $I = 150$. As we know, the location of the equilibrium changes as you slide I up and down. Check that the middle "branch" of the bifurcation diagram tracks the voltage of the equilibrium. The color coding tell us about the stability of the equilibrium. What does black mean? What does red mean?

(1.6.2) Now let us consider the the two green (upper and lower) voltage levels on the bifurcation diagram at $I = 150$. What do they represent? If it is not clear from the phaseplane, use the graph of voltage versus time to confirm that they correspond to the maximum and minimum voltage levels of the stable limit cycle corresponding to tonic spiking. As with the equilibrium, check that the green branches of the bifurcation diagram track the voltage extremes of the stable limit cycle (and action potentials) as you slide I up and down.

Unstable limit cycle. We are ready to examine the bifurcations underlying the sudden appearance and disappearance of stable limit cycles we observed in Section 1.5. To fix ideas, consider the region of the bifurcation diagram between $I = 235$ and $I = 238.5$, where the stable limit cycles disappear. The blue points in this region represent the maximum and minimum voltage levels of an *unstable* limit cycle. The unstable limit cycle is like an offstage Shakespearean actor. We will see how it is "born" in a *Hopf bifurcation* at the equilibrium, and "dies" in a *saddle-node bifurcation of limit cycles* taking the stable limit cycle with it.

Hopf bifurcation. The bifurcation diagram shows us that at the exact value of I where the unstable equilibrium regains stability (turning from black to red on the diagram, around $I = 235$), a small unstable limit cycle is "born" around the equilibrium. The unstable nature of the equilibrium has been passed off to the new cycle. This creation of a limit cycle as an equilibrium changes stability is called a *Hopf bifurcation*. For a small range of subsequent values of I, the large stable limit cycle coexists with the small unstable limit cycle, so there is a stable equilibrium and *two* limit cycles: one stable and one unstable. Over the next few exercises, we will confirm this in XPP, and use a sneaky trick to plot the unstable limit cycle.

(1.6.3) According to the bifurcation diagram, the equilibrium regains stability at about $I = 235$, and we know from Section 1.5 the stable limit cycle disappears just before $I = 239$. So choose the intermediate value $I = 237$. Erase everything (*e*), plot the nullclines (*n*,*n*), and choose

an initial condition like (−60,0) to see the stable limit cycle. Zoom in (*(W)indow/zoom, (Z)oom In*) so that the limit cycle fills the view. Erase everything again (*e*), redraw the nullclines (*n,n*), and choose *(I)nitialconds, (L)ast* so that the last point computed at the end of the last trajectory is used as the initial condition for the next trajectory. Since the last point was very close to the stable limit cycle, this should yield a clean picture of the cycle.

(1.6.4) We will use XPP's graphics tools to "freeze" this clean picture of the stable limit cycle for $I = 237$. Click *(G)raphics stuff, (F)reeze*, and then *(F)reeze* again. At the color prompt, choose 7, for green, to be compatible with the bifurcation diagram. (The default color, 0, is black, 1–10 range thru shades of red, orange, yellow, green, blue and purple, in that order.) Choose "stable" for the name and key. Now, whenever you erase everything, if you click *(R)estore*, the frozen cycle will re-appear. (You can change the color and name, add a key, or unfreeze the cycle, using *(E)dit, (K)ey* and *(D)elete* respectively in the *(G)raphics stuff, (F)reeze* menu.)

(1.6.5) Click *i, i* to choose initial conditions with the mouse. Choose an initial condition inside and close to the stable limit cycle, to confirm that it is, indeed, stable. (Note that choosing the initial condition on one of the nullclines can help you keep track of where you started.) Now, choose another initial condition inside the stable limit cycle, but close to the equilibrium this time. If you are close enough, the trajectory will spiral in toward the equilibrium, confirming its stability. We have just shown that the system is *bistable*, meaning that the long-term behavior depends critically on the choice of initial condition. The unstable limit cycle acts as a threshold, also known as a *separatrix*, between the two modes of behavior. Try different initial conditions to get a sense of where the unstable limit cycle must be. (Remember to click the *escape* key to liberate your mouse when you are done.)

Plotting the unstable limit cycle. Here is the sneaky trick we will use: What would happen to a trajectory that spirals away from the unstable limit cycle and toward the stable equilibrium if we could run it *backward* in time? It would spiral *away* from the equilibrium and *toward* the limit cycle. "Backwards" time is surprisingly easy to implement for an autonomous system of differential equations; we just make the time step negative.

(1.6.6) In XPP, click *u* for *N(u)merics*, then *d* for the time step, *Dt*. The XPP command line will show the current value of *Dt*. Edit the command line (you can use the arrows on your keyboard) to put a negative sign in front of the value, and click the *return* key. Click the *escape* key to exit the numerics menu. Now, XPP will run time backward. Choose an initial condition that spiraled in to the equilibrium in the previous exercise, and

watch the unstable limit cycle appear. For a clean picture of the unstable cycle, erase everything (*e*), redraw the nullclines (*n,n*), and choose the last point computed as the new initial condition (*i,l*). Freeze the unstable limit cycle (*g,f,f*) using color 9, for blue, and "unstable" for the name. Now, when you click *(R)estore*, both limit cycles should re-appear.

(1.6.7) Check that the voltage extremes of the two limit cycles agree with those given by the bifurcation diagram for $I = 237$ in Figure 1.6.

(1.6.8) While we are working with backward time, let us slide I to see the Hopf bifurcation in action. Change the I slider to range from 230 to 238. Click *n(U)merics, (T)otal* to change the total run time to 2500 in the XPP command line, to give trajectories more time to settle down in this delicate region. Warning: increasing the run time slows XPP down, so it is a good idea to change it back to 500 at the end of this section. Remember to click the *escape* key to exit from the numerics menu. Confirm that when $I = 230$, the equilibrium is unstable (i.e., stable in this backward time). Now, slowly increase I, to watch the birth of a limit cycle at the equilibrium, and the gradual growth of the limit cycle as I increases to 238. This limit cycle is stable in backwards time, so unstable in forward time. Use *Restore* to compare limit cycles for different values of I with the frozen limit cycles for $I = 237$.

(1.6.9) Exactly which part of the bifurcation diagram was Exercise 1.6.8 about? Take a moment to clearly describe the correspondence between the bifurcation diagram and your XPP results.

(1.6.10) Now, we will focus on the "fold" in the bifurcation diagram where the blue branch representing the unstable limit cycle meets the green branch representing the stable limit cycle. Continuing in backwards time mode, set the I slider to range from 237 to 238.35. Slide I up and watch the unstable limit cycle continue to grow as I increases. Freeze the unstable cycle for $I = 238.35$. Next we will compare it to the stable limit cycle for $I = 238.35$. Go back into the *n(U)umerics* menu, and make *Dt* positive so that time is running forwards again. (Remember to click on *escape* to exit the numerics menu.) Restore all the saved cycles, set $I = 237$, choose an initial condition on the stable limit cycle, and slowly slide I up to 238.35 again to watch the stable cycle shrink as I increases. Notice that the stable and unstable limit cycles are much closer together when $I = 238.35$ than they were when $I = 237$. it is not a coincidence that we chose the value $I = 238.35$ so carefully. If you try repeating this exercise for $I = 238.5$, you will find the limit cycles have disappeared.

Saddle-node bifurcation of limit cycles and the offset of tonic spiking. In the last exercise, we saw the two limit cycles converging to each other as I was increased, exactly as predicted by the bifurcation diagram. In the thin region between the pair of limit cycles, trajectories spiral outward.

Outside that region, trajectories spiral inward. The limit cycles separate the inward and outward cycling behavior. As the two limit cycles converge, the region between them shrinks to nothing, till the limit cycles coalesce and disappear, and all trajectories spiral inward. This convergence and disappearance of a pair of limit cycles is called a *saddle-node bifurcation of limit cycles*, and corresponds to the sudden offset of tonic spiking in the voltage trace. (The word *saddle* denotes the unstable limit cycle, while *node* denotes the stable limit cycle. The naming scheme seems strange, but originates from analogy with the *saddle-node bifurcation of equilibria* that we will see in Sections 1.7 and 1.9.)

Onset of tonic spiking. The sudden onset of tonic spiking in our simulated current clamp experiment of Section 1.5 is also associated with an unstable limit cycle that is born in a subcritical Hopf bifurcation and dies in a saddle-node bifurcation of limit cycles. But the sequence of events is slightly different. The birth of the unstable limit cycle as the equilibrium gains stability, and the converge and disappearance of the limit cycles, all happen as I is decreased rather than increased. In our simulated current clamp experiment, I was increased, so there was a spontaneous creation of a pair of limit cycles that appeared to come from nowhere, out of the "clear blue sky." This explains why a saddle-node bifurcation of limit cycles is sometimes called a *blue sky bifurcation*.

Subcritical versus supercritical Hopf bifurcations. The type of Hopf bifurcation exhibited by this system, where an unstable limit cycle is born, is called *subcritical*. There are also *supercritical Hopf bifurcations* in which a stable limit cycle is born as the equilibrium changes stability. Here, the word *critical* refers to the value of the bifurcation parameter where the equilibrium changes stability and the limit cycle is born. *Subcritical* and *supercritical* describe which side of that critical value the limit cycle is born into: as an unstable limit cycle surrounding the stable equilibrium (subcritical) or as a stable limit cycle surrounding the unstable equilibrium (supercritical).

In real applications, when a subcritical Hopf bifurcation occurs it is often paired with a saddle-node bifurcation of limit cycles (the large stable limit cycle maintains the large-scale stability of the system, so that trajectories do not grow without bound). In the bifurcation diagram, this manifests as the (blue) branch of unstable limit cycles, born at the Hopf bifurcation, appearing to "fold back" on itself, changing stability in the process. Thus, the saddle-node bifurcation of limit cycles is also called a *fold bifurcation of limit cycles*, and the pair of bifurcations is sometimes collectively referred to as a *backward Hopf bifurcation*.

Supercritical Hopf bifurcations are simpler to understand: the birth and growth of the limit cycle are observable (without resorting to backward time), and the oscillations grow gradually as the bifurcation parameter is varied, rather than appearing out of the blue. See, for example, the models of calcium driven oscillations in Chapter 3.

(1.6.11) Let us put it all together! Revisit the simulated current clamp experiment of Section 1.5, and explain how you can use the bifurcation diagram to predict the model cell's response to sustained current (the sequence of voltage traces and phase-plane portraits, and the associated values of I in Figure 1.5).

(1.6.12) Now, we will focus more closely on the appearance of tonic spiking, to investigate some consequences of bistability. Delete all the frozen trajectories (*g,f,d*) and return the phase plane to default size (*w,d*). Check the total run time is still 2500 (using *n(U)merics, (T)otal*, and the command line; remember to click the *escape* key to exit the numerics menu). Reset the initial condition to (−60,0) to represent the cell at rest before any current is applied (using *IC's* button). Set the I slider to range from 90 to 105, and confirm that, with this initial condition, tonic spiking appears around $I = 96$, as in (Figure 1.5). Exactly which part of the bifurcation diagram does this represent? The point to notice is that from the initial condition (−60,0), the trajectory "discovers" the stable limit cycle as soon as the blue sky bifurcation has occurred.

(1.6.13) What if the cell's history meant that it was starting at a different initial condition? For example, set the initial condition to $(V, W) = (-25, 0.15)$. Now, slide I again, from 90 to 105. When does the trajectory discover the stable limit cycle? You should find that it is different from the previous exercise. Why is that? Exactly which part of the bifurcation diagram does this represent? The initial condition (−25,0.15) was carefully chosen so that as I is increased, the cell stays quiescent, tracking the equilibrium voltage as long as the equilibrium point is stable, and happily oblivious of the "blue sky" bifurcation creating the pair of limit cycles. It is only when the equilibrium point loses stability at the Hopf bifurcation, around $I = 102$, that trajectories are forced to discover the large, stable limit cycle and the cell starts tonic spiking.

Bistability means history matters. For a parameter value where the system is bistable, such as $I = 98$, there are two *attractors* (in this case the stable equilibrium and the stable limit cycle). Each attractor has a *basin of attraction*, consisting of all the initial conditions it attracts. The basin of attraction of the stable limit cycle consists of all the initial conditions leading to tonic spiking, while the basin of attraction of the stable equilibrium consists of all the initial conditions leading to quiescence. The threshold, or *separatrix*

between the two basins of attraction is the unstable limit cycle. Bistability means that we cannot predict the cell's behavior without knowing its recent history, since the history sets the initial condition. In Exercise 1.6.12, the initial condition represents a history of a cell at rest until a current step (from $I = 0$) is applied. In contrast, a cell *in vivo* may experience a slowly changing stimulus, more akin to a slow ramp of applied current, such as the slow modulation of calcium sensitive channels by slow accumulation of cytosolic calcium discussed in Chapters 3 and 4. If the stimulus current changes slowly enough, relative to the phase-plane dynamics, the cell can track the slowly changing stable equilibrium, resulting in a history that is better approximated by the initial condition of Exercise 1.6.13 than that of Exercise 1.6.12. These subtleties of multi-stability combined with time-scale separation are key to models of bursting.

Bifurcation and bursting. Now that we know how to read the bifurcation diagram, we can use it to predict the results of a fixed current injection, or of a slowly changing stimulus current. The bifurcation diagram predicts the sudden appearance and disappearance of large amplitude tonic spiking, including the subtleties of bistability associated with the cell's history. In Section 1.10, bursting behavior is modeled by adding a slowly changing variable, intrinsic to the cell, that drives the cell back and forth across bifurcations in a multistable regime, thereby "switching" tonic spiking on and off.

Plotting bifurcation diagrams. By now, you may be wondering how we (or the computer) establish the stability of the equilibrium or limit cycle with precision, and how we plot the bifurcation diagram. Section 1.11 is about how to determine stability. The bifurcation diagram was plotted using XPP's interface with the bifurcation software AUTO (indy.cs.concordia.ca/auto) in the *File* menu. Learning to use AUTO is exciting, but is beyond the scope of this tutorial. Our experience is that it works well to have an expert show you how to get started, then carefully follow the AUTO tips on Ermentrout's XPP help pages (Ermentrout, 2012) to build on that foundation.

Different bifurcations yield different spiking characteristics. In the next sections, we will see how manipulating the parameters of K-channel gating within the Morris–Lecar model yields two more bifurcation mechanisms for the onset of tonic spiking, each leading to different spiking characteristics. In the example we just worked through, tonic spiking was restricted to a narrow frequency range, as in Hodgkin's Class II, resonator, neurons (Hodgkin, 1948). The *SNIC bifurcation* in the next section yields tonic spiking with arbitrarily low frequency, depending on applied current, as in

Hodgkin's Class I, integrator, neurons. The *Homoclinic bifurcation* in Section 1.9 yields tonic spiking with a high baseline between the spikes. This collection of bifurcation mechanisms provides building blocks for modeling the rich diversity of cellular excitability, and biological oscillations more generally. See introductory textbooks on dynamical systems, such as Blanchard *et al*. (2011), Ellner and Guckenheimer (2006), Hirsch *et al*. (2012), and Strogatz (1994) for more introduction to bifurcations, and Bertram *et al*. (1995), Ermentrout and Terman (2010), Golubitsky *et al*. (2001), and Izhikevich (2007) for approaches to classifying bifurcations in the context of excitable systems.

1.7 Saddle node on an invariant circle (SNIC) bifurcation

Different cell types, ion channels, and conditions correspond to different ranges of parameter values. For example, recall that V_3 represents the half-activation voltage of the inhibitory conductance, and increasing V_4 decreases the slope of the conductance curve at half-activation. These gating parameters vary enormously between channel types and cells, and are easily shifted by mechanisms like phosphorylation, G-protein binding and steroid binding (Carrasquillo and Nerbonne, 2014; González *et al*., 2012; King *et al*., 2006; Lovell *et al*., 2000, 2001; Pongs and Schwarz, 2010; Vacher and Trimmer 2011). Temperature can dramatically impact gating kinetics, captured in the model by ϕ (Hille, 2001), and the maximal conductances, g_{Ca},g_K, and g_L depend on the number and density of channels expressed, which vary widely between and within cells, as well as on single-channel conductance.

In this section, we will work with the SNIC parameter set of Table 1.1, which differs only in the voltage dependence of potassium-channel gating from the Hopf parameter set of the preceding sections. Our parameter choices are similar to choices often used in the literature, going back (in nondimensionalized form) to Rinzel and Ermentrout (1989) and to some extent to Morris and Lecar (1981). There is nothing extraordinary about the exact values, in the sense that nearby parameter values yield similar behavior. Sliders in XPP can be used to explore the *sensitivity* of the behavior to parameters (how much each parameter can change before a new bifurcation occurs).

(1.7.1) Set up XPP with a phase-plane window and a voltage trace window (as in Exercise 1.5.2), and change the total run time back to 500, if necessary (*u,t*). Select the SNIC parameter set using *(F)ile, (G)et par set*. Open the parameter window (using the *param* button at the top of the XPP window), enlarge it to see all the parameters, and check that they agree with the SNIC column of Table 1.1. Only the parameters V_3 and

V_4 have changed; perhaps representing a different K channel. What do the new parameters say about the voltage-dependent gating of the new channel compared to the old?

(1.7.2) Let us see what effect the new parameters have on the nullclines and equilibria of the system. Set up sliders for V_3 and V_4 so that each varies between the Hopf and SNIC values (Table 1.1), and plot the nullclines. Recall from Section 1.4 that the W nullcline is simply the graph of $W_\infty(V)$, the K-channel open probability at steady state as a function of V. Is this consistent with the way the nullcline changes as you slide V_3 and V_4? By contrast, the V nullcline does not change with V_3 and V_4. Look back at Equation (1.22) for the V nullcline to see why: V_3 and V_4 play no role in the equation.

(1.7.3) Set V_3 and V_4 at their SNIC values (12 and 17, respectively). When $I = 0$ the nullclines intersect three times, representing three equilibria. Click on some initial conditions close to each equilibrium (using *i,i*) to determine whether they are stable. Or quickly sample the behavior in the whole phase plane using the flow (*(D)ir. field/flow, (F)low*, with a 10×10 grid). Despite the new equilibria, the behavior is much the same as before. There is one stable equilibrium, giving a resting potential of approximately -60, and almost all initial conditions settle down to rest, either directly, or after the transient excursion of a single action potential.

(1.7.4) Activate the voltage trace window and simulate a sustained current injection experiment (as in Section 1.5), with the initial condition set at $(V, W) = (-60, 0)$ to represent a cell at rest before the current is applied. A good range for I is -25 to 150. The voltage response shows many similarities with the behavior in Section 1.5: as you increase I, rest gives way to tonic spiking, and eventually the spiking disappears in damped oscillations to plateau voltage. What are some differences from the behavior in Section 1.5? Check the onset of spiking carefully. Notice that there are no lone action potentials; the cell snaps straight from rest to tonic spiking. If you slide I delicately, you may be fooled into thinking you have found a lone action potential (around $I = 39.75$), but if you extend the t axis to 1000 ms and continue the run (click *(C)ontinue* and choose run time 1000 in the command line), you find that it is really very low frequency tonic spiking. From there, the spike frequency increases rapidly with increasing I, so that small changes in I lead to dramatic frequency modulation.

(1.7.5) Now, watch the onset of spiking in the phase plane. What is going on? At $I = -25$ there is only one equilibrium. As you increase I, a pair of new equilibria are created when the V nullcline "pushes through" the W nullcline. So there are three equilibria by the time I reaches 0, as we know from Exercise 1.7.3. What happens to the middle equilibrium as

you continue to increase I? It travels down the nullclines to coalesce and vanishes with the lower equilibrium when the V nullcline pushes through the W nullcline again. At exactly that moment, the stable limit cycle appears. This is not a coincidence.

(1.7.6) To understand how the stable limit cycle appears as the nullclines push through each other, it is helpful to focus on each of the two equilibria that coalesce and vanish together. Set $I = 27$, where there are three fairly evenly spaced equilibria. Zoom in closely on the lower equilibrium (click *(W)indow/zoom, (Z)oom in*, then use the cursor to select a very small box around the equilibrium). Erase (*e*) and redraw the nullclines (*n,n*) for accuracy at this scale, then plot the flow using *(D)ir field/flow, (F)low* and a 10×10 grid. If you zoomed in closely enough, it should look like Figure 1.7e. The equilibrium is asymptotically stable, meaning all nearby trajectories converge to it. There is also a pattern to the convergence. All the trajectories swoop around and approach the equilibrium along one of two directions, and those two directions line up along a single line. A stable equilibrium with this pattern of convergence along a line (rather than around a full spiral) is called a *stable node*. Nodes can be stable or unstable. An *unstable node* is like a stable node running in reverse time. See Section 1.11 for more detail about how we classify equilibria.

(1.7.7) Next, we will zoom in on the upper equilibrium. Return to the default phase-plane window size (*w,d*), erase everything and redraw the nullclines. Zoom in on the upper equilibrium and plot the flow to get something like Figure 1.7g. These trajectories are truly spiraling, and get crowded, so we used a 6×6 grid for the figure. Click on some initial conditions to confirm that the equilibrium is unstable. An equilibrium with trajectories spiraling away like this is called an *unstable spiral*. An equilibrium with trajectories spiraling in is called a *stable spiral*.

(1.7.8) Now, let us zoom in on the middle equilibrium. Once again, return to the default phase-plane window size (*w,d*), erase everything, and redraw the nullclines. Zoom in on the middle equilibrium, redraw the nullclines, and plot the flow to get something like Figure 1.7f. This time we used a 15×15 grid for the figure to emphasize the pattern. The tractories swoop toward the equilibrium from one direction, and away from the equilibrium in another direction. Click on some initial conditions to check which direction is "in" and which direction is "out." Pay particular attention to the diagonal line that separates trajectories swooping to the right from trajectories swooping to the left. A trajectory exactly on the diagonal line swoops neither left nor right, but instead converges directly to the equilibrium. This line is called the *stable manifold* of the equilibrium. There is another line separating trajectories coming from above versus below the equilibrium. A trajectory exactly on this line comes from neither above nor below. It comes directly

from the equilibrium. In other words, in *backward* time, it converges directly to the equilibrium. This line is called the *unstable manifold* of the equilibrium. An equilibrium like this, with a stable manifold and an unstable manifold, is called a *saddle*. It is unstable, since most trajectories end up swooping away from it.

(1.7.9) Let us zoom back out again to see how these local pieces are globally connected. In particular, where do the trajectories on the unstable manifold of the saddle end up in forward time? It is hard to plot the exact trajectories, but choosing any initial conditions very close to the saddle, just to the right and just to the left, shows us what happens. The left branch of the unstable manifold converges directly to the stable node, while the right branch takes an excursion corresponding to a single action potential before settling down to the stable node (Figure 1.7a, top). Each branch of the unstable manifold consists of a *heteroclinic connection*, meaning a trajectory that connects two equilibria. Taken together, the two heteroclinic connections form a loop in phase plane. This loop is key to the SNIC bifurcation underlying the onset of tonic spiking in this section.

Invariant circle. The loop described in the previous exercise is the *invariant circle* of the *saddle node on an invariant circle bifurcation*. Here, the word *circle* is used loosely, to mean a closed loop, rather than a perfectly round circle. (In other words, it is used in the topological rather than geometric sense.) The word *invariant* refers to the fact that the circle is invariant under the flow, meaning that it is composed of trajectories of the flow.

Saddle-node bifurcation of equilibria. Each time the nullclines push past each other, a saddle and a node (either stable or unstable) coalesce and disappear in a *saddle-node bifurcation of equilibria*. This is often referred to, simply, as a *saddle-node bifurcation*, and is the *saddle node* of the *saddle node on an invariant circle bifurcation*. Viewed the other way around, each time the nullclines meet and push through each other, a pair of equilibria (one saddle and one node) are created in a saddle-node bifurcation. (The node may than evolve into a spiral as the equilibria separate, as in Exercise 1.7.7.) See Section 1.11 for more detail.

Saddle node on an invariant circle (SNIC) bifurcation. We are now ready to view the SNIC bifurcation as a saddle-node bifurcation of equilibria occurring along an invariant circle. On the short branch of the invariant circle in Exercise 1.7.9, between the two equilibria, the flow is clockwise. On the long branch, the flow is counterclockwise. As I is increased, the saddle and the stable node converge, and the short, clockwise branch of the invariant

circle shrinks. At the moment of the saddle-node bifurcation, the clockwise branch of the invariant circle vanishes. What remains is a counterclockwise invariant circle with a single equilibrium. As I is further increased, the equilibrium vanishes and the invariant circle becomes a stable limit cycle, inheriting the stability of the old node (Figure 1.7a, middle and bottom). Thus, at exactly the moment when the V nullcline pushes through the W nullcline, the cell starts tonic spiking.

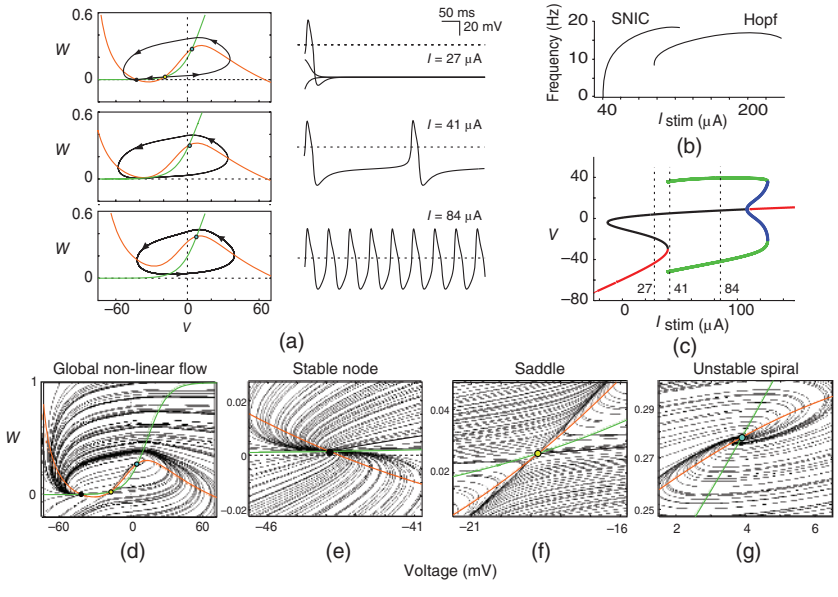

Figure 1.7 Sustained current injection with the SNIC parameter set. (a) Series of phase-plane trajectories and corresponding voltage traces obtained with the stimulus current amplitudes indicated. For $I = 27$ μA, there are three equilibria (at the nullcline intersections). The two branches of the unstable manifold of the (middle) saddle equilibrium follow different trajectories (one sub- and one super-threshold) to the stable node, forming a "circle." As I increases, the nullclines separate and the equilibria are lost from the circle, transforming it into a stable limit cycle. Firing begins at very low frequency when the limit cycle is first created, because the motion slows almost to a stop, in memory of the lost equilibria. As the nullclines separate further, firing frequency increases. (b) Firing frequency plotted against stimulus amplitude, for the SNIC and Hopf parameter sets. The two parameter sets differ only in the voltage dependence of K-channel gating, but the associated bifurcations yield behaviors exemplifying Hodgkin's excitability Classes I and II, respectively: firing frequency starts low and grades up smoothly with increasing current in the SNIC example, but is narrowly constrained in the Hopf example. (c) Bifurcation diagram, charting the equilibria and limit cycles from each phase plane, as in Figure 1.6. The SNIC bifurcation occurs just below $I = 41$ μA, where the large stable limit cycle is created at the moment the stable equilibrium is lost in a saddle-node bifurcation. The termination of firing follows the same bifurcation structure as in the Hopf example. (d) Flow in the phase plane when $I = 27$ μA, with enlargements. (e–f) Detailed flow structure close to each equilibrium.

(1.7.10) Figure 1.7c shows the bifurcation diagram for I ranging from -25 to 150. As usual, there is a lot of information packed into the diagram. Take some time to read it carefully. Which parts of the diagram correspond to the pairwise appearance and disappearance of equilibria? Which parts correspond to the stable node, saddle and unstable spiral? What color is the saddle, and why? Where is the SNIC bifurcation? Why does the end of the green branch representing the stable limit cycle line up with the fold in the middle branch? Finally, use the bifurcation diagram to explain the results of your simulated current injection experiment, including both the appearance and disappearance of tonic spiking.

(1.7.11) Why do the spikes first appear with such low frequency, as shown in Figure 1.7a and b? Hint: plot the (unscaled) direction field as you slide I through the SNIC bifurcation. Do you see the "ghost" effect of the vanished equilibria, slowing the motion on their stretch of the limit cycle? This ghost effect explains why the SNIC bifurcation yields Hodgkin's Class I, integrator neurons. Check the voltage trace again to confirm this is consistent with the waveform, and explain why the spike frequency increases as I increases.

Hodgkin's classification of neurons. In Figure 1.7b, spike frequency is plotted against applied current for the SNIC and Hopf parameter sets. Rinzel and Ermentrout (1989) describe how the associated bifurcations correspond to the characteristics of Hodgkin's Class I and Class II neurons (Hodgkin, 1948). In the SNIC bifurcation, tonic spiking appears with arbitrarily low frequency, as in Hodgkin's Class I, so the neuron has the capacity to be integrative, in the sense that the voltage response is graded with the strength of the stimulus. By contrast, in the saddle-node bifurcation of limit cycles (paired with the subcritical Hopf bifurcation), tonic spiking occurs over a very narrow frequency range, as in Hodgkin's Class II, so the neuron has the capacity to resonate with a specific stimulus frequency. See Izhikevich (2007) for a fuller characterization of classes of excitability.

1.8 Time-scale separation

Our final parameter set ("Homoclinic" in Table 1.1) differs from the SNIC parameter set only in the kinetics of K-channel gating. The parameter ϕ is increased in Equation (1.13), so that K channels respond more quickly to voltage change. In Section 1.9, we simulate a current clamp experiment and study the associated bifurcations for this parameter set. But first we explore the impact of changing the time scale of W, relative to that of V, on the overall dynamics of the system. Time-scale structure is a powerful

point of contact between biology and mathematics. There is a vast range of time scales in biology, and the level of Time-scale separation between variables has important consequences for model behavior and analysis.

(1.8.1) Set up XPP with a phase-plane window and voltage trace window (as in Exercise 1.5.2). Adjust the phase-plane window (using *(V)iewaxes*) so that W ranges from -0.2 to 0.6. Set the initial condition to $(V, W) = (-60, 0)$, the total run time to 500 (using *u,t*), and I to 0. Choose either the SNIC or homoclinic parameter set (using *(F)ile, (G)et par set*), and check Table 1.1 to confirm that the only difference between these two parameter sets is the value of ϕ. Create a slider for ϕ that ranges between the two values, from 0.04 to 0.22. Plot the nullclines (*n,n*) and slide ϕ. Why are the nullclines unchanged? One way to explain it is by noticing that ϕ does not appear in either of the nullcline Equations (1.19) and (1.22). Now, explain it in terms of the the meaning of ϕ for K channels.

(1.8.2) Even though changing ϕ does not change the nullclines, it has a dramatic effect on the behavior of the system. Turn on the scaled direction field (using *d,s*) and slide ϕ. As ϕ increases, the arrows all get steeper. Why? First, let us think about it in terms of the equations. Recall from Section 1.4 that the slope of each arrow is given by its "rise/run," where the rise is the rate of change dW/dt in the W direction, and the run is the rate of change dV/dt in the V direction. Look back at Equations (1.12) and (1.13) for dV/dt and dW/dt. What role does ϕ play in each equation? How does this explain what happens to the slopes of the arrows as ϕ increases? Now explain it in terms of the meaning of ϕ.

(1.8.3) What impact do you predict the increase in ϕ will have on spike waveform and frequency?

(1.8.4) Let us test your prediction. Set I to 42 and ϕ to 0.04. Sketch the nullclines to confirm this is just after the SNIC bifurcation of Section 1.7. Plot the voltage trace, and with the voltage trace window active, gradually slide ϕ up to 0.22. Is this what you predicted? When ϕ is small, spike frequency is low: the model K channels open slowly, so the voltage reaches a high peak before the K current catches up. Similarly, the K current drives the voltage to a deep hyperpolarization before the channels have slowly closed. Higher values of ϕ represent K channels that open and close more quickly. Thus, the voltage peaks earlier, does not hyperpolarize so deeply, and the spike frequency increases. The high spike baseline is particularly striking. We will return to this feature in Section 1.10 when we extend the Morris–Lecar model to exhibit bursting.

(1.8.5) Now let us return to the phase plane and direction field to see what is going on. Plot the trajectory (*i, g*), and the scaled direction field (*d,s*). When $\phi = 0.04$, we recognize the large limit cycle resulting from the SNIC bifurcation in Section 1.7. Gradually increase ϕ, and notice how the direction field steepens, causing the limit cycle to narrow in the V

direction and elongate in the W direction. As you further increase ϕ, the limit cycle shrinks toward the equilibrium.

(1.8.6) Expand the ϕ slider to range from 0.01 to 0.5, to exaggerate the geometric phenomenon at play here. See Figure 1.8. As we change ϕ, the relative time scales of V and W change. When $\phi = 0.01$, V is much faster than W, the direction field is almost horizontal in most of the plane, and the flow is dominated by the fast change in V. It is only when dV/dt is close to 0, in the neighborhood of the V nullcline, that W, the slow variable, has much impact on the direction field and flow. As ϕ is increased to intermediate values, the V and W time scales become more similar, and the slopes in the direction field are more varied and less extreme. When ϕ reaches 0.5, W has become the fast variable, and the direction field is almost vertical in most of the plane.

Fast/slow dynamics. Notice how the shape of the limit cycle is tightly controlled by the folded shape of the V nullcline when V is the fast variable ($\phi = 0.01$) (see Figure 1.8a). On the "bottom" stretch of the limit cycle, the fast V dynamic "whisks" the trajectory to the right branch of the V nullcline. Now, the slow W dynamic comes into play. dW/dt is positive, albeit small, so the trajectory slowly climbs up the V nullcline, while the V dynamic ensures the trajectory "hugs" the nullcline tightly. At the nullcline's "knee", the fast V dynamic takes over again, whisking the trajectory

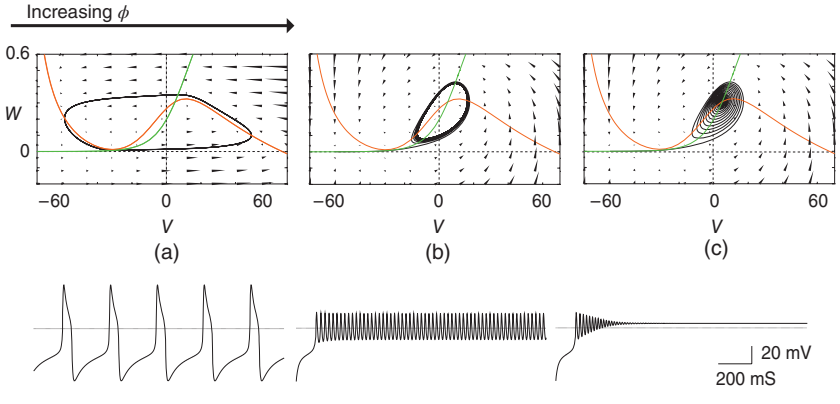

Figure 1.8 Changing time-scales. Only the rate constant of K-current activation, ϕ, is varied between the graphs, so the nullclines do not change. All other parameters are from the SNIC parameter set, as in Figure 1.7, with I held constant at 42 μA. Arrowheads represent the direction field. (a) $\phi = 0.01$, so W changes slowly relative to V. The direction field is primarily horizontal, and the large limit cycle (resulting from a SNIC bifurcation) hugs the V nullcline more tightly than in Figure 1.7, where $\phi = 0.04$. (b) $\phi = 0.22$. W changes on a similar time scale to V, and the cycle has a dramatically different shape, corresponding to low amplitude spikes with a high baseline. (c) $\phi = 0.23$. The cycle has disappeared altogether, so the spikes damp down to the attracting equilibrium.

over to the left branch of the nullcline, where dW/dt is negative, and so the cycle continues. This interaction between nullcline geometry and fast/slow separation of time scales has generated a rich body of mathematical research (see, for example (Jones, 1995) and (Zeeman, 1977)).

(1.8.7) Plot the voltage trace for $\phi = 0.01$ and describe how each of the fast and slow components of the limit cycle in the phase plane correspond to features of the voltage waveform. You can add extra detail by thinking about the location of the equilibrium, and the "ghost" of the SNIC bifurcation, relative to the limit cycle.

Time-scale separation and model reduction. Recognizing the separation of time scales and how they relate to your time scale of interest can be helpful for model simplification, as we will see throughout the book. For example, our model assumption that Ca channels activate instantly is a statement about the relative time scales of Ca-channel activation, K-channel activation, and action potentials in our model cell.

Time-scale separation and bursting. Separation of time scales also underlies many models of bursting. The basic idea is that a third variable with a time scale that is slow compared to both V and W, repeatedly tips the system across bifurcations from equilibrium to cycling and back. In Chapters 3 and 4, for example, calcium build up plays the role of the slow variable. If the third time scale is slow enough, the system tips between "hugging" the equilibrium and hugging the limit cycle, in much the same way as it hugs the two slow branches of the nullcline in Figure 1.8. In Section 1.10, we extend the Morris–Lecar model with a slow variable to illustrate the idea. To prepare for this, in Section 1.9, we study the homoclinic bifurcation mechanism that underlies the onset of high baseline spiking.

1.9 Homoclinic bifurcation

Figure 1.9a shows the bifurcation diagram when we set $\phi = 0.22$ (the "Homoclinic" parameter set in Table 1.1) and vary I to simulate a sustained current injection experiment. Comparing it with the previous two bifurcation diagrams, we see interesting similarities and differences. For example, there is a region of *tri-stability*, between $I = 37.2$ and $I = 39.6$, where two stable equilibria and a stable limit cycle co-exist. See Figure 1.9e–g for the case $I = 38$. You can use techniques from the previous sections to explore the phase plane and voltage traces, unpacking all the information in the bifurcation diagram. The following exercises focus on the differences from the SNIC example in the onset of spiking.

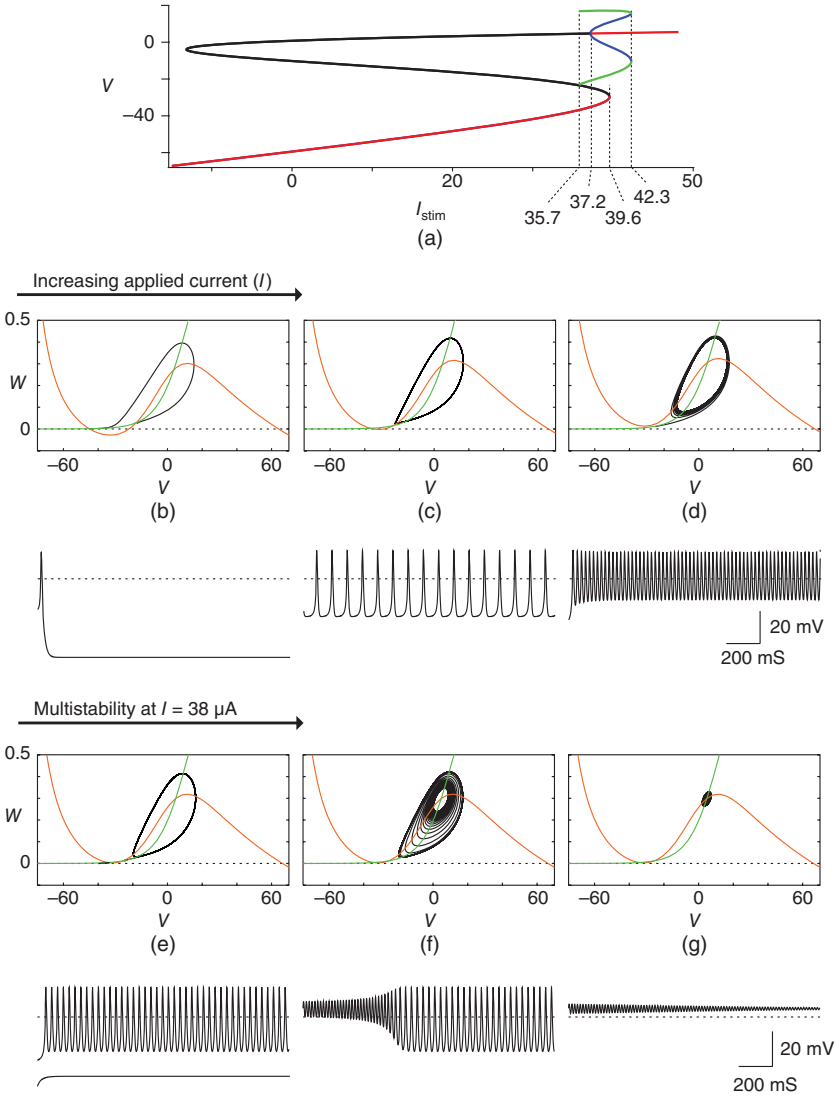

Figure 1.9 Sustained current injection with the Homoclinic parameter set. (a) Bifurcation diagram, showing the homoclinic bifurcation at $I = 35.7$ μA, and subsequent regions of bi- and tri-stabilities. (b–d) Phase-plane trajectories and nullclines and corresponding voltage traces as applied current is increased through the bifurcation. Notice the graded firing frequency response and the high spike baseline corresponding to the limit cycle position. Viewed from (d) to (b), the stable limit cycle grows till it collides with the saddle equilibrium to become a homoclinic loop and disappear in the homoclinic bifurcation. (e–g) Tri-stability when $I = 38$ μA. There is a stable limit cycle (e and f), with (e) a stable equilibrium outside and (f) a stable spiral equilibrium inside.

(1.9.1) Continuing from Section 1.8, check the total run time is still 500 (*u,t*, and remember to *escape* from the numerics menu). Select the Homoclinic parameter set (*f, g*), and restrict the ϕ slider to range from 0.04 to 0.22 again. Set I at 42, plot the trajectory (with initial condition (−60,0)), and slide ϕ between the two extremes. Recall from Section 1.7 that when $\phi = 0.04$, the limit cycle is created by a SNIC bifurcation, so the limit cycle follows the shape of the SNIC invariant circle, enclosing the delicate region where the nullclines almost touch. As ϕ is increased, the limit cycle passes through that delicate region. This is our hint that when we fix ϕ at 0.22, and slide I in a simulated current injection experiment (as in Sections 1.5 and 1.7) we should expect to see a slightly different bifurcation mechanism for the onset of tonic spiking.

(1.9.2) Let us try it. Set $\phi = 0.22$, add a slider for I ranging from −25 to 50, and explore what happens in the phase-plane and voltage trace windows as you slide I.

(1.9.3) As I increases, the pairwise appearance and disappearance of equilibria as the nullclines pass through each other should look familiar: it is exactly the same as in the SNIC bifurcation. Why? (For a hint, look back at Exercise 1.8.1. By contrast, the limit cycle and tonic spiking look quite different from those in the SNIC example.

(1.9.4) As with the SNIC bifurcation in Section 1.7, the stable equilibrium is lost when the stable node and the saddle coalesce and disappear, around $I = 40$. But this time the stable limit cycle appears far from the saddle-node bifurcation. What happened to the invariant circle of the SNIC example? To answer this, begin by setting $I = 27$, plot the flow (using *d, f* with a 10×10 grid), and compare it with the flow in Figure 1.7d. Describe some of the differences.

(1.9.5) Erase the flow (*e*), replot the nullclines (*n. n*), and choose an initial condition just to the right of the saddle equilibrium (*i, m*) to approximate the right-hand branch of the unstable manifold of the saddle (see Exercises 1.7.8 and 1.7.9 to review stable and unstable manifolds). Notice how the unstable manifold returns fairly close to the saddle, from above, before heading over to the stable equilibrium, as shown in Figure 1.9b.

(1.9.6) Reset the I slider to range from 27 to 50, and gradually increase I. What happens to the unstable manifold of the saddle? Just before $I = 36$, it returns to become the stable manifold of the same saddle! See Figure 1.9c. A trajectory like this, that starts and ends at the same saddle, is called a *homoclinic loop*.

(1.9.7) Continue to increase I. The homoclinic loop disappears, giving birth to a stable limit cycle in its wake (Figure 1.9d). This is a *homoclinic bifurcation*. The unstable manifold of the saddle now spirals into the stable limit cycle. Set $I = 37$, and plot the entire flow again (*d, f* with a 10×10 grid) to see that the system is now bistable. There is a stable equilibrium around

$V = -35$, and the new stable limit cycle. Choose initial conditions in the phase plane (i, i) to plot the corresponding voltage traces (rest, and tonic spiking, respectively) for each stable state. (Remember you can turn simplot on (m,s) to plot the phase plane and voltage trace simultaneously.) Use the phase plane to explain why the spike baseline is so high, above the resting potential.

(1.9.8) It can be easier to understand the homoclinic bifurcation by considering what happens to the stable limit cycle as I *decreases* through the bifurcation value $I \approx 35.7$. To explore this, zoom in (w,z) on the region of the phase plane containing the action (the equilibria and the limit cycle). Set the I slider to range from 34 to 41, and position it at $I = 41$. Choose an initial condition inside the stable limit cycle, and within the basin of attraction of the limit cycle, so it spirals out to the cycle. (Note, from the bifurcation diagram, that the equilibrium inside the limit cycle is also stable when $I = 41$, and there is an unstable limit cycle separating the basins of attraction of the stable limit cycle and the equilibrium. Try a few initial conditions inside the stable limit cycle to check this, and to find one that spirals out to the stable cycle.) Now, gradually decrease I, and watch what happens to the stable limit cycle and the equilibria.

Homoclinic bifurcation: a limit cycle collides with a saddle equilibrium. In Exercise 1.9.8, the stable limit cycle steadily grows as I is decreased. Around $I = 39.6$ the nullclines touch, and a saddle and stable node appear. As I continues to decrease, the stable limit cycle and saddle move inexorably towards each other. The *homoclinic bifurcation* is the moment of collision, when the limit cycle becomes a homoclinic loop, and vanishes. This viewpoint of bifurcations occurring when limit sets collide can help bring clarity to several of the bifurcations we have encountered where equilibria or limit cycles seem to appear out of "thin air."

Saddle-node bifurcation: a stable node and saddle collide. Every intersection of the nullclines is an equilibrium, and a saddle-node bifurcation occurs every time the nullclines push through each other. Depending on the direction that I is varied, a saddle-node bifurcation can be viewed as the creation of a saddle and node pair of equilibria where the nullclines first touch, or as the collision and disappearance of a saddle-node pair as the nullclines push past each other. In a bifurcation diagram, a saddle-node bifurcation appears as a fold in the branch of equilibria, as in Figures 1.7c and 1.9a. For this reason, it is also called a *fold bifurcation*.

SNIC bifurcation: a limit cycle collides with a degenerate equilibrium. In the SNIC bifurcation of Section 1.7, a saddle-node collision of equilibria occurs on

the invariant circle as I is increased. Viewed from the other direction, as I is decreased, the limit cycle collides with an equilibrium at the moment of a saddle-node bifurcation. In other words, a homoclinic bifurcation occurs simultaneously with a saddle-node bifurcation. The equilibrium is called degenerate at that moment, because it is neither a saddle nor a node, but a hybrid of the two.

Saddle-node bifurcation of limit cycles: stable and unstable limit cycles collide. In Exercises 1.6.6–1.6.10, we saw an unstable cycle that was born at the equilibrium (in a Hopf bifurcation) grow inexorably till it collided with a stable limit cycle and the two cycles disappeared in a saddle-node bifurcation of limit cycles. In our bifurcation diagrams, a saddle-node bifurcation of limit cycles appears as a fold in the branch representing limit cycles, emphasizing the similarity with the saddle-node bifurcation of equilibria.

(1.9.9) Exactly where, on the bifurcation diagram (Figure 1.9a), is the homoclinic bifurcation? Why does the green branch representing the stable limit cycle end abruptly when it meets the black branch? What does that black branch represent? What does the fold in the black/red branch at $I = 39.6$ represent? What does the fold in the blue/green branch at $I = 42.3$ represent? (Hint: review Exercise 1.6.10).

(1.9.10) Use the same carefully chosen initial condition as in Exercise 1.9.8 to watch what happens to the voltage trace as you decrease I from 41, and the limit cycle approaches the saddle. The spike frequency decreases dramatically, as in the SNIC example and Hodgkin's Class I neurons. Why?

(1.9.11) Reset the initial condition to $(-60, 0)$, gradually increase I from 34, and watch what happens to the voltage trace again. Use the bifurcation diagram to explain why the tonic spikes appear with high frequency, instead of the low frequency we observed in the previous exercise.

Bifurcations switch spiking on and off. This completes our tour of parameter space for the Morris–Lecar model. It is by no means exhaustive. Indeed, we have only used three of an infinite choice of parameter sets. Nevertheless, we hope it has conveyed some of the richness of behavior of the model, and of the associated bifurcation mechanisms that switch spiking on and off with different characteristics of excitability. In the next section, we continue to follow Rinzel and Ermentrout (1989), using the Homoclinic parameter set to explore how a cycle of bifurcations, repeatedly switching spiking on and off again, can be used to model intrinsic bursting behavior.

1.10 Bursting

In this section, we extend the Morris–Lecar model to illustrate how bursting can arise as a slow passage, back and forth, across bifurcations from rest to spiking. For a range of stimulus currents, I, the homoclinic parameter set of the last section exhibits multiple stable modes of behavior, including rest and tonic spiking. Moreover, the different modes of behavior have voltage separation, in the sense that the spike baseline is above the resting potential. This creates an opportunity for the different behaviors to feed back and control the stimulus current via voltage, sweeping I back and forth across the bifurcations.

(1.10.1) To fix ideas, consider the homoclinic bifurcation diagram in Figure 1.9a, and suppose $I = 38$ (Figure 1.9e–g). Depending on the cell's history, it may be resting or spiking. If it is at rest, at the lower stable node, what happens if I gradually increases (in other words, if I is driven to the right on the bifurcation diagram)? We know from the diagram, and from our simulated current injection experiments, that the cell will track the stable node until it disappears in the saddle-node bifurcation. Then the cell will suddenly start spiking.

(1.10.2) Now, suppose the cell is spiking. What happens if I gradually *decreases* (i.e., is driven to the left on the bifurcation diagram)? We can read the diagram, or revisit Exercise 1.9.8 to answer this. The cell will continue to spike, tracking the limit cycle, until the cycle collides with the saddle and disappears. Then the cell will suddenly return to rest.

Voltage-dependent slowly varying current. From Exercises 1.10.1 and 1.10.2, we see that if I is driven to the right (increases) when the cell is at rest, but is driven to the left (decreases) when the cell is spiking, the cell will tip back and forth between rest and spiking, in a classic bursting fashion, as in Figures 1.1 (data) and 1.10 (model). In the model, the voltage separation between the resting and spiking states means that voltage feedback can be used to drive I in opposite directions during rest versus spiking. Let us translate this into a differential equation. The cell will burst if:

- the rate of change of I is positive when V is low (at resting levels), and
- the rate of change of I is negative when V is high (at spiking levels).

To clarify what we mean by "low" and "high" voltage levels, let V_b denote a voltage level between the resting and spiking levels. Check the bifurcation

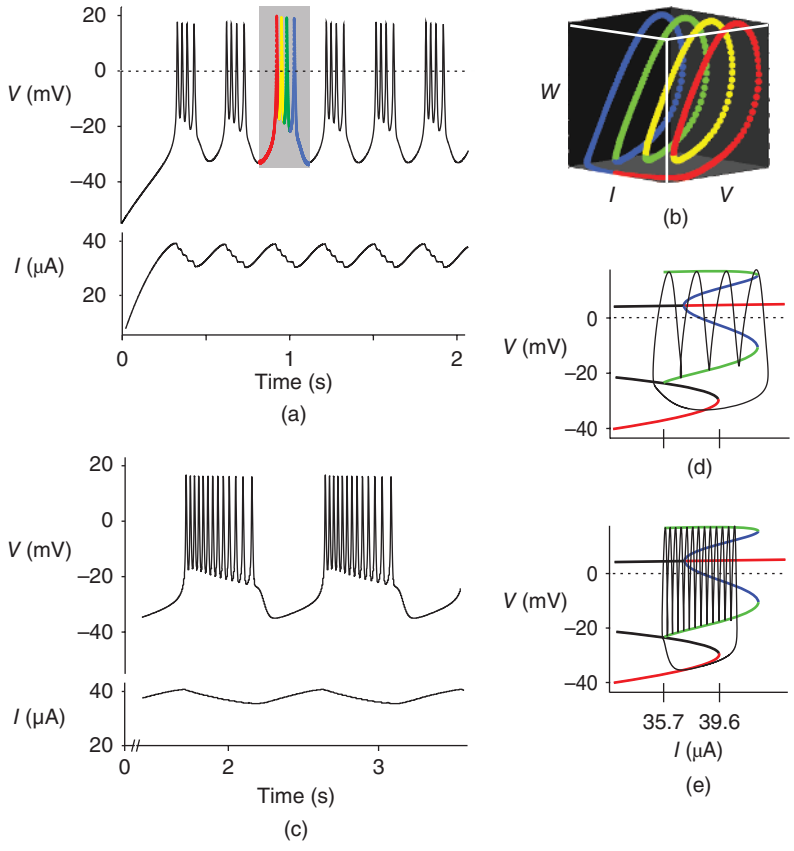

Figure 1.10 Bursting in the extended Morris–Lecar model. Starting with the homoclinic parameter set, internal voltage-dependent kinetics are included for the applied current, so that I slowly increases when $V < -20$ and slowly decreases when $V > -20$. (a) Burst firing, with rate constant $r = 0.005$ for I kinetics. Behavior of the added current is shown below the voltage trace. Gray highlight indicates the recurring cycle encompassing one burst. (b) The corresponding burst trajectory is a limit cycle in three-dimensional phase space. Each burst corresponds to a complete passage around the cycle. Individual spikes within the burst are colored as in A. The spike waveforms change slightly during a burst, but the burst as a whole follows the recurring cycle. (c) Longer bursts with more spikes are elicited when the added current, I, changes even more slowly ($r = 0.001$). (d and e) Details of the bifurcation diagram from Figure 1.9 onto which a two-dimensional projection of the three-dimensional burst cycles in (b) and (c), respectively, are superimposed. The projection is the view from directly "above" the cycle in (b), looking down on the I–V plane. During the interburst interval, $V < -20$ so I slowly increases, sweeping to the right on the bifurcation diagram. During this quiescent state, the cell tracks the low voltage stable equilibrium on the bifurcation diagram. When I passes 39.6 μA, the stable equilibrium disappears in a saddle-node bifurcation, and the cell, seeking an alternative stable state, jumps to the stable limit cycle and starts spiking. With the increase in voltage, I changes direction to decreasing, slowly sweeping to the left. The cell continues to spike, tracking the stable cycle until the cycle collides with the saddle and disappears in a homoclinic bifurcation when $I = 35.7$ μA. The cell is forced to seek the quiescent state again, the voltage drops, and the entire burst cycle repeats. The slower rate constant of I in (e) means there is less "momentum" (greater Time-scale separation), and the trajectory hugs the bifurcation diagram more closely.

diagram to confirm that we could, for example, choose $V_b = -25$ mV. Then, the cell will burst if

$$\frac{dI}{dt} > 0 \qquad \text{when} \qquad V < V_b, \quad \text{and} \tag{1.23}$$

$$\frac{dI}{dt} < 0 \qquad \text{when} \qquad V > V_b \tag{1.24}$$

(1.10.3) Confirm that, for positive values of r, conditions (1.23) and (1.24) are satisfied by the differential equation

$$\frac{dI}{dt} = r(V_b - V) \tag{1.25}$$

We will examine the role of r in Equation (1.25) in the XPP exercises below.

Extended Morris–Lecar model. Recall that the Morris–Lecar model we have been exploring is defined (mathematically) by Equations (1.12)–(1.16), in which I is treated as an externally varied parameter. In the XPP program *BridgingTutorial-Burst.ode* (available online or from the authors), we extend the model with Equation (1.25), so that I is now treated as an intrinsic variable, with V, W, and I all feeding back on each other, either directly or indirectly. Equation (1.25) is somewhat abstract, in the sense that it was chosen for its simplicity, and is not modeling a specific physiological mechanism for slowly varying I. Physiological mechanisms that have an analogous effect on current would also promote bursting. See Chapters 3 and 4 for calcium-induced bursting, and Bertram *et al.* (1995), Ermentrout and Terman (2010), and Golubitsky *et al.* (2001), Izhikevich (2007) for surveys and classifications of bursting mechanisms.

Three-dimensional systems. The extended Morris–Lecar model is three dimensional, in the sense that it has three dependent variables (V, W, and I). Instead of a phase *plane*, there is a three-dimensional phase *space*. As with the phase plane, a set of initial conditions $V(0), W(0)$, and $I(0)$ corresponds to a point in phase space. Given the initial conditions, iteratively computing the future values of $V(t), W(t)$, and $I(t)$ may take a bit more computer time than for two variables, but is not conceptually different. The trajectory followed by $V(t), W(t)$, and $I(t)$ is a curve weaving around in three-dimensional phase space, instead of a two-dimensional plane. There *is* a conceptual difference here. Recall from Section 1.4 that trajectories cannot cross each other. In two dimensions, this has restrictive consequences. For example, a trajectory that starts inside a limit cycle can never get outside. Not so, in three dimensions! What does "inside" a limit cycle even mean in three dimensions? There is plenty of

room for trajectories to weave around and around themselves and each other. Try "googling" *strange attractor*, and choosing *images*, to see some of the extraordinary and beautiful paths trajectories can take in three dimensions. The equations behind those images can be remarkably simple; see textbooks on dynamical systems and chaos, such as Blanchard *et al.*, (2011), Hirsch *et al.* (2012), and Strogatz (1994), to learn more.

(1.10.4) Returning to our extended Morris–Lecar model, look over the XPP program *BridgingTutorial-Burst.ode*. Find the parts of the code that correspond to:

- The new differential equation for I.
- The way that V feeds back into I.
- The way that I feeds back into V.
- The default initial conditions for V, W, and I.
- The new parameters r and V_b.
- The default parameter set being used.
- The total run time being used.
- The default window view that XPP will open to.

(1.10.5) Open XPP using *BridgingTutorial-Burst.ode*. It should open to a voltage trace window, with $r = 0.01$, $V_b = -20$, the homoclinic parameter set, and initial conditions $(V, W, I) = (-60, 0, 0)$. Run it (using *i,g*). You should see bursting behavior, similar, but not identical, to Figure 1.10a. Describe some of the differences from Figure 1.10a.

(1.10.6) Open a second window (using *m, c*), and plot the time course of I (using *Viewaxes*, or *Xi* versus *t* and the command line). Confirm that, as we planned, I increases when the cell is quiescent (at rest), and decreases when the cell is spiking. Why does I have a "sawtooth" shape? To answer this, look back at each of the terms in Equation (1.25), and the voltage trace.

(1.10.7) Use Equation (1.25) and the bifurcation diagram (Figure 1.9a) to explain why I and V steadily climb from their initial conditions until the bursting starts.

(1.10.8) Now, let us examine the role of r in Equation (1.25). What do you predict will happen if we decrease r? Create a slider for r, ranging from 0.001 to 0.01, and try it. Is it what you predicted? As you decrease r, I changes more slowly. So it takes longer for I to drive the cell from one bifurcation to the other, and back again. Thus, the burst frequency decreases. (Burst frequency means the number of entire bursts per time unit.) Near $r = 0.006$, it takes I so long to drive the cell through the spiking regime, that the cell suddenly increases to 4 spikes per burst, instead of 3.

(1.10.9) Why does the spike frequency decrease within each burst? And why does the spike baseline decrease within each burst? Hint: which

bifurcation terminates the burst? Think about what is going on in the V-W phase plane.

(1.10.10) As you continue to decrease r, the bursts take longer, and the number of spikes per burst continues to increase. Why does it also take so much longer for the first burst to get started?

(1.10.11) Figure 1.10 shows several views of the bursting behavior at $r = 0.005$ and $r = 0.001$. When $r = 0.005$, the cell fires 4 spikes per burst (Figure 1.10a). Each spike represents a circuit around the slowly growing stable limit cycle in the slowly evolving V-W phase plane of Section 1.9, while each burst represents a circuit around the bifurcation diagram (Figure 1.10d). Let us isolate one burst. First, zoom into the voltage trace (*w,z*) to confirm that there is a complete burst between 900 ms and 1200 ms. We will select that burst. In the *n(U)merics* menu, set the *(T)otal* run time to be 1200 (use the command line, and remember to type *return*). Then set the *t(R)ansient* time to be 900. Click on *escape* to exit the numerics menu. Erase everything (*e*), return the window to default size (*w, d*) and plot the single burst (*i, g*). Use *(V)iewaxes* to view the burst in lots of different ways. We have already seen V versus t and I versus t. What about W versus t? Or V versus W? Or V versus I? Or W versus I? In each case, make a prediction first. Good ranges for the axes are V: -40 to 30, I: 30 to 50, W: -0.2 to 1, and t: 900 to 1200.

(1.10.12) Let us view the burst in three dimensions. First we will view the time course of V and W changing together. Click *(V)iewaxes, (3)D*, and choose t for the X-axis, V for the Y-axis, and W for the Z-axis. You do not need to fill in the ranges, but be sure to fill in the last three boxes with the axis labels (t, V, and W). When you click *OK*, you may be presented with a blank screen. Fear not! Click *(W)indow/zoom, (F)it*, and your three-dimensional plot should appear. You can rotate the image by holding the mouse down and moving the cursor. Experiment with the rotation, to get "end on" views that look like your two-dimensional plots from the previous exercise, and "diagonal" views that show how the two dimensional plots (*projections*) relate to each other in three dimensions. (Use *(W)indow/zoom, (F)it* again if the image rotates out of view).

(1.10.13) Now, let us view the burst in I, V, W space, to reproduce Figure 1.10b. This is the *phase space* for the system; the three dimensional analogy of a two dimensional phase *plane*. It gives a beautiful view for understanding how the each burst corresponds to passage around a coiled, three-dimensional limit cycle. This limit cycle in phase space traces a circuit, tracking the stable equilibrium of the two-dimensional system during quiescence (as I increases), and the stable limit cycle of the two-dimensional system during spiking (as I decreases), thereby forming a loop as I slowly varies back and forth. Rotate this image to make sure that you see how to relate the full, three-dimensional loop

to the two-dimensional projection of the loop in the V versus I plot. Note that you may need to change the order of V and W (and their axes labels) in *(V)iewaxes, (3)D* to get the views you want.

Visualizing bursting on the bifurcation diagram. Of the two-dimensional plots, V versus I is particularly informative, because V measures the behavior of the cell, and I is the bifurcation variable. Indeed, the V versus I plot has the same axes as the bifurcation diagram, so the two are often superimposed, as in Figure 1.10d and e. There is some subtlety (slight of hand, even) to appreciate here. The bifurcation diagram is about the stable sets in the two-dimensional V, W phase plane *with I held constant*, for each value of I. The superimposed burst trajectory is about the path followed by V and W *when I is slowly varying*. If I slowed down all the way to a *stop*, the bifurcation diagram could tell us about the exact (deterministic) behavior of V and W for the value of I where we stopped. When I is varying, the bifurcation diagram tells us the approximate behavior of the trajectory. The slower I varies, the more closely the trajectory follows the bifurcation diagram. Compare Figure 1.10 parts D ($r = 0.005$) and E ($r = 0.001$). When I changes more slowly ($r = 0.001$), the burst trajectory "hugs" the stable branches of the diagram, and the bifurcations themselves, more closely.

1.11 Eigenvalues and stability

Throughout the tutorial, we have seen the importance of stability for understanding and predicting the behavior of a model. So far, we have used simulations to determine the stability properties of limit sets (equilibria and limit cycles), we have worked with bifurcation diagrams that informed us of the stability properties, and we have noticed that changes in stability are associated with bifurcations. We close the tutorial by returning to the two-dimensional Morris–Lecar model, to describe how the stability properties of an equilibrium can be characterized by its *eigenvalues*. Recall that stability is about the behavior of trajectories close to the equilibrium. The essential idea of this section is *linearization* of the system close to the equilibrium. In other words, close to the equilibrium we approximate the nonlinear system with something linear (and, therefore, simpler), and deduce the stability properties from the approximation.

One-dimensional linear differential equation. We will start by developing intuition for one of the simplest, but most useful, differential equations out there:

$$\frac{dx}{dt} = kx \tag{1.26}$$

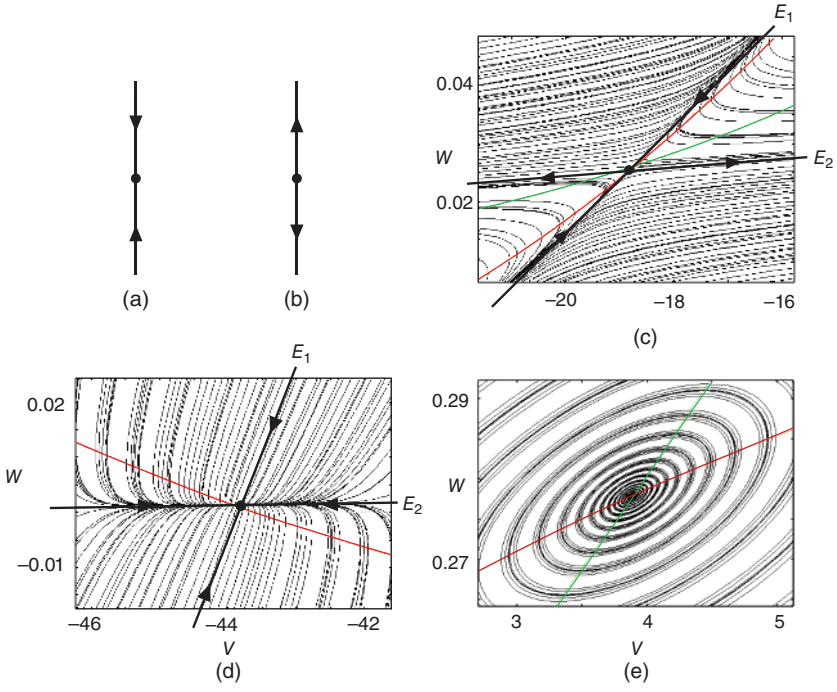

Figure 1.11 Eigenvalues and stability. (a and b) An equilibrium of a linear one-dimensional dynamical system has a single eigenvalue, indicating the direction and rate of flow (towards or away from the equilibrium). The eigenvalue is (a) negative when the equilibrium is stable and (b) positive when the equilibrium is unstable. (c–e) Magnified view, close to an equilibrium in a two-dimensional system. The equilibrium has two eigenvalues, organizing the direction of flow. (c) A saddle has one negative and one positive eigenvalue corresponding to flow towards and away from the saddle along eigendirections E_1 and E_2, respectively. (d) A stable node has two negative eigenvalues, $k_1 < k_2$, corresponding to flow along eigendirections E_1 and E_2, respectively. (e) A spiral equilibrium has complex eigenvalues (a complex conjugate pair). The equilibrium is unstable when the real part of the eigenvalues is positive, stable when the real part of the eigenvalues is negative. Parameter values given in the text.

Equation (1.26) is *one-dimensional*, because there is only one equation, and one variable x. There is also one parameter, k. Equation (1.26) is called *linear*, because the right-hand side, kx is a linear function of x. Recall that when we had two equations for two variables, V and W, we plotted the trajectories in a two-dimensional phase plane. When we extended the Morris–Lecar system to three equations, for the three variables V, W, and I, we plotted the trajectories in three-dimensional phase space. Equation (1.26) has one variable, so we plot the trajectories on a one-dimensional *phase line* as shown in Figure 1.11a and b.

(1.11.1) We have not yet said what the variable x represents. For now, let us simply say x measures position on the phase line. Imagine yourself

as an ant, living a one-dimensional life on the phase line. Suppose that x denotes your position, and Equation (1.26) determines your motion. Consider the case when $k = 2$.

- Which direction do you (the ant) walk from initial position $x = 3$?
- Which direction do you walk from initial position $x = -3$?
- Which direction do you walk from initial position $x = 0$?
- Which phase line shows your motion, Figure 1.11a or Figure 1.11b?

If $x > 0$, then $kx > 0$ (since $k = 2$), so $dx/dt > 0$, and you walk in a positive direction, further away from $x = 0$. Similarly, if $x < 0$, then $dx/dt < 0$, and you walk in a negative direction from your negative initial position. In other words, you walk further way from $x = 0$ again. If you start at exactly $x = 0$, then $dx/dt = 0$, so you do not move. In summary, when $k = 2$, $x = 0$ is an unstable (repelling) equilibrium, corresponding to Figure 1.11b.

(1.11.2) What if $k = -2$? There is an equilibrium at $x = 0$ again. Which direction do you walk from initial position $x = 3$ this time? And which direction from initial position $x = -3$? Confirm that, wherever you start, you head "home" to $x = 0$. So, when $k = -2$, $x = 0$ is a stable (attracting) equilibrium, corresponding to Figure 1.11a.

(1.11.3) What if $k = -1$? The phase line will look the same as for $k = -2$, but there is a difference. Do you head home to $x = 0$ faster when $k = -2$ or when $k = -1$?

(1.11.4) How do the cases $k = 1$ and $k = 2$ compare? In both cases, you are repelled from $x = 0$. Is the repulsion stronger when $k = 1$ or when $k = 2$?

The sign of k determines attraction versus repulsion. Summarizing, when k is positive in Equation (1.26), the equilibrium at $x = 0$ is repelling, and when k is negative, the equilibrium is attracting. The larger the magnitude of k, the stronger the attraction or repulsion. If we now think of x as representing displacement from the equilibrium at $x = 0$, then k characterizes the feedback of x onto itself. When $k < 0$, there is negative feedback, the displacement decays and we return to equilibrium. When $k > 0$, there is positive feedback and the displacement grows (exponentially). Equipped with this intuition for the one-dimensional flow of Equation (1.26) along a line, we now return to the two-dimensional Morris–Lecar model.

(1.11.5) Open XPP with *BridgingTutorial-MLecar.ode*, and choose the SNIC parameter set (*f,g*). Set $I = 27$ as in Exercises 1.7.6–1.7.9, and plot the global non-linear flow (using *d, f,* and a 10×10 grid), as in Figure 1.7d. We will focus on the saddle equilibrium first (Figure 1.7f). Recall that the saddle has a stable manifold and an unstable manifold, composed of trajectories. The two branches of the unstable manifold "emerge" directly

from the saddle, and take different routes to the stable node (creating the invariant circle of the SNIC bifurcation). The two branches of the stable manifold head directly into the saddle. One branch emerges from the unstable spiral, the other comes from below. Close to the saddle, all other trajectories are guided towards the saddle by the stable manifold, swoop past, and are guided away again by the unstable manifold.

(1.11.6) Repeat Exercise 1.7.8, to zoom into a neighborhood of the saddle, as in Figures 1.7f and 1.11c. When you zoom in closely enough, the stable and unstable manifolds look like straight lines. Remind yourself which straight line is the stable manifold, and which is the unstable. If the flow does not happen to show the unstable manifold clearly (it depends where the grid of initial conditions falls), remember that you can plot a good approximation by choosing initial conditions with the mouse (*i, i*) just to the left and right of the saddle.

(1.11.7) Now repeat the process to zoom in even more closely, choosing a small box around the saddle within the already zoomed-in window. Replot the nullclines and flow. Do you see any difference? It should look like Figure 1.7c again, except the scale on the axes is finer. Do it again. And again. It still looks just like Figure 1.7c. If you keep zooming, you will find your computer's limits. But until that point, we are seeing fairly compelling evidence that no matter how closely we look, the flow close to the saddle is organized by the same two straight lines. These straight lines are called *eigendirections*. The eigendirections are *tangent* to the stable and unstable manifolds at the saddle point: the more closely we zoom in, the straighter the manifolds look, and the more closely they are approximated by the eigendirections. "Eigen" is a German word for "self." Why do you think it is used in this context? Flow on an eigendirection flows along itself. It is just flow along a straight line.

(1.11.8) Flow along a straight line is like flow in one dimension. In fact, it is a (mathematically proven) theorem that when we zoom in closely enough, the flow along an eigendirection is well approximated by $dx/dt = kx$ for the right choice of constant k. This theorem is key to how we quantify stability, so let us work with it. Imagine ignoring all of the phase plane except the attracting eigendirection (the line E_1 in Figure 1.11c). Along E_1, the flow is directed toward the saddle. Let x denote the distance from the saddle along the line E_1, positive x going up and to the right, negative x in the opposite direction. The saddle is at $x = 0$, so the flow is directed toward $x = 0$ from both sides. Is this reminding you of the ant in Exercises 1.11.1–1.11.4? What sign does k_1 have to be, for $dx/dt = k_1 x$ to give a good approximation to the flow on the attracting eigendirection? The number k_1 is called the *eigenvalue associated with the eigendirection* E_1.

(1.11.9) What role does the size of the eigenvalue play? Which would correspond to stronger attraction to the saddle along the attracting eigendirection, $k_1 = -2$ or $k_1 = -1/2$?

(1.11.10) Now, let us think about the repelling eigendirection (the line E_2 in Figure 1.11c), and let x denote distance from the equilibrium along E_2. What sign would k_2 have to be for $dx/dt = k_2 x$ to give a good approximation to the flow on the repelling eigendirection? In other words, what sign is the eigenvalue corresponding to the repelling eigendirection?

(1.11.11) What role does the size of the eigenvalue play in the repelling case? Which would correspond to stronger repulsion from the saddle, $k_2 = 2$ or $k_2 = 1/2$?

(1.11.12) Recall that changing ϕ changes the slopes in the direction field, but does not change the locations of the nulllclines or the equilibria. Change ϕ to 0.22 (as in the homoclinic example). Confirm that the flow around the saddle is organized by two eigendirections again, with one positive eigenvalue and one negative. How can you tell that k_1 is stronger relative to k_2 than it was for $\phi = 0.04$?

A saddle has eigenvalues of opposite signs. Let us review the overall saddle behavior again: trajectories are carried in toward the equilibrium by the eigendirection with a negative eigenvalue, and carried out again by the eigendirection with a positive eigenvalue. This is true for every saddle in the phase plane. Indeed, one way to define a saddle equilibrium is that it has one positive and one negative eigenvalue. Notice that one positive eigenvalue is enough to make an equilibrium unstable. Almost every trajectory is carried away by it.

(1.11.13) Let us apply the same way of thinking to the stable node. With $\phi = 0.22$ and $I = 27$, return to the default window size in XPP (using *w, d*), then zoom into the stable equilibrium. Once again, if you keep zooming in, you find the flow always looks the same. And once again, the flow is organized by two straight line eigendirections E_1 and E_2, as in Figure 1.11d. Explain how we know that the corresponding eigenvalues k_1 and k_2 are both negative.

(1.11.14) In the example of the previous exercise (Figure 1.11d), which eigenvalue has the larger magnitude, k_1 or k_2? In other words, is the attraction stronger along E_1 or E_2? This can be somewhat counter intuitive, so let us think carefully about it. The two eigendirections collaborate to guide trajectories toward the equilibrium, by guiding them toward each other. Attraction along E_1 guides trajectories toward E_2. Similarly, attraction along E_2 guides trajectories toward E_1. The fact that trajectories swoop first toward E_2 tells us the attraction *toward* E_2 is stronger than

the attraction *along* E_2. In other words, E_1 is the stronger eigendirection, and k_1 has the larger magnitude.

Nodes have eigenvalues of the same sign. A stable node has two negative eigenvalues, corresponding to a flow organized by two attracting eigendirections. An unstable node is like a stable node running in reverse time: it has two positive eigenvalues, corresponding to a flow organized by two repelling eigendirections.

(1.11.15) Now, let us focus on our third equilibrium, the unstable spiral. Continuing with $\phi = 0.22$ and $I = 27$, return to the default window. Zoom into the unstable spiral, redraw the nullclines, and plot the direction field with a 2×2 grid so the phase plane is not too densely filled. Zoom in again. The flow looks the same as you keep zooming in (see Figure 1.11e), but there are no eigendirections!

Spiral equilibria have complex eigenvalues. Spiraling flow is incompatible with straight lines. Nevertheless, there are still eigenvalues associated with spiraling into, or out of, an equilibrium, and the intuition we developed with straight lines can still help. The eigenvalues for a spiraling equilibrium are complex numbers, of the form $\alpha + i\beta$, where $i = \sqrt{-1}$. We call α the *real part* of the complex number, and β the *imaginary part*. Moreover, the eigenvalues for a spiral equilibrium are closely related: if $k_1 = \alpha + i\beta$, then $k_2 = \alpha - i\beta$ (that is, the eigenvalues form a *complex conjugate pair*). The real part of the eigenvalues matches our straight line intuition, and tells us about the attraction or repulsion of the equilibrium. If $\alpha < 0$, the equilibrium attracts, and the trajectories spiral inward. If $\alpha > 0$, the equilibrium repels, and the trajectories spiral outward. The imaginary part of the eigenvalues tells us about the rate of rotation around the equilibrium as the trajectory spirals in or out. If you have not thought about complex numbers recently (or ever), you can read about them on the web, or in an introductory textbook on differential equations, such as Blanchard *et al.* (2011). The essential message, for our immediate purposes, is that the real part of the eigenvalues tells us about the stability of the equilibrium.

(1.11.16) Equilibrium points are also called *singular points*. The *(S)ing pts* menu in XPP is worth exploring. Let us try it on the unstable spiral. Return to the default window, click on *(S)ing pts, (M)ouse*. A tiny window will open, instructing you to click where you guess there is a singular point. Click near the unstable spiral. A new tiny window will open asking whether to print eigenvalues. Choose *(Y)es*. Three things happen simultaneously:

- A square appears in the phase plane, marking the unstable spiral.

- The eigenvalues are printed in the XPP console window. Confirm that they are of the form $\alpha + i\beta$ and $\alpha - i\beta$ (approximately $0.016 \pm i0.036$).
- Another small window opens, titled "Equilibria." At the top of this window, we are told this equilibrium is *Unstable*. The middle of the window tells us the stability-relevant properties of the eigenvalues. For example, $c+ = 2$ tells us there are two complex eigenvalues with positive real part, so we know the equilibrium is an unstable spiral. Note that r stands for real eigenvalues (with imaginary part $\beta = 0$) and *im* stands for purely imaginary eigenvalues (with real part $\alpha = 0$). The bottom of the window shows the V, W coordinates of the equilibrium.

(1.11.17) We are currently using the homoclinic parameter set. Recall from the bifurcation diagram in Figure 1.9a that there is a Hopf bifurcation around $I = 37.2$. Before the bifurcation, the equilibrium is an unstable spiral (as in the previous exercise), so has eigenvalues with positive real part. After the bifurcation the equilibrium is a *stable* spiral, so the eigenvalues have negative real part. How does the transition from positive to negative real parts happen? To see how this works, set up a slider for I ranging from 27 to 40, and use the *(S)ing pts* menu to print the eigenvalues for different values of I as you cross the bifurcation. For example, try $I = 32$, $I = 35$, $I = 36$, $I = 37$, $I = 37.1$, $I = 37.2$, $I = 38$, $I = 39$, and $I = 40$. As you vary I through the Hopf bifurcation, the complex parts of the eigenvalues do not change much, but the real parts of the eigenvalues get smaller and smaller in magnitude until they pass through zero as they change from positive (unstable spiral) to negative (stable spiral).

At a Hopf bifurcation, the equilibrium has purely imaginary eigenvalues. In other words, the real part of the eigenvalues is zero. This is a powerful statement. Indeed, it is how we define the bifurcation. When the real part of the eigenvalues passes through zero, the equilibrium changes stability. If we can compute eigenvalues, we can locate the bifurcation.

Calculating eigenvalues. In this tutorial, we use XPP to compute eigenvalues. Most introductory texts in differential equations, dynamical systems or mathematical biology describe how to calculate eigenvalues directly from a model's differential equations. For example, see Blanchard *et al*. (2011), Edelstein-Keshet (2005), Ellner and Guckenheimer (2006), Hirsch *et al*. (2012), and Strogatz (1994). It is a two-step process. The first step is *linearization*: using calculus to find the best linear approximation to the non-linear system, close to the equilibrium of interest. In other words, formalizing our process of zooming-in to each equilibrium. The second step is to calculate the eigenvalues of the linearization, using matrix algebra. For two-dimensional systems, it is a fairly straightforward process,

and eigenvalues can often be calculated by hand. For models with more variables, we are more likely to use the computer.

(1.11.18) Reset $I = 27$, and try the *(S)ing pts* menu on the saddle. Confirm that

- The saddle is marked with a triangle in the phase plane.
- The eigenvalues (shown in the console window) are real numbers with opposite signs, as expected.
- The "Equilibria" window tells us this is an unstable equilibrium with one positive real eigenvalue ($r+ = 1$), and one negative ($r- = 1$).

Another tiny window opens for the saddle. XPP is offering to draw the *invariant sets*, meaning the stable and unstable manifolds of the saddle. Choose *(Y)es*. There are four branches to be drawn, and you need to click *escape* after each branch, to plot the next one. The unstable branches are drawn first, in "gold," taking their two different routes to the stable equilibrium. Next come the stable branches, one emerging from the unstable spiral, the other coming from below. (Note that, in truth, the four branches meet at the saddle, but in practice XPP plots them slightly offset.)

(1.11.19) What will XPP tell you about the stable node? Try it. As expected, the eigenvalues are both negative. Recall from Exercise 1.11.14 that we know the stronger eigenvalue corresponds to the "strong" eigendirection, E_1 (so $k_1 = -0.588$), and the weaker eigenvalue corresponds to the "weak," roughly horizontal eigendirection, E_2 (so $k_2 = -0.074$). A tiny window opens offering to draw the *strong sets*. Choose *(Y)es*. This time there are two branches to be drawn (and you need to click *escape* after each one). The strong set of a stable node is composed of trajectories that approach the stable node directly along the strong eigendirection. (All the other trajectories approach the node along the weak eigendirection.)

(1.11.20) Recall from the bifurcation diagram in Figure 1.9a that the saddle and stable node coalesce and disappear in a saddle-node bifurcation around $I = 39.6$. How does an equilibrium whose eigenvalues have opposite signs coalesce with an equilibrium with two negative eigenvalues? Print the eigenvalues for the two equilibria for different values of I to see how this works. (It will go more quickly if you decline the offer to draw invariant sets and strong sets.) For example, try $I = 37$, $I = 38$, $I = 39$, $I = 39.3$, and $I = 39.5$. It may help to zoom into the region where the two equilibria coalesce. As the equilibria converge, their eigenvalues also converge. In particular, the positive eigenvalue of the saddle and the weak eigenvalue of the stable node each converge to zero.

Locating bifurcations At the saddle-node bifurcation, the equilibrium has one negative eigenvalue and one zero eigenvalue. Once again, this is a powerful

statement. If we can compute the eigenvalues, we can locate the bifurcation. These ideas recur throughout the book. You will see many discussions of real eigenvalues passing through zero, or complex eigenvalues crossing the imaginary axis (meaning that the real parts pass through zero). They signal bifurcations, where interesting or surprising qualitative changes in behavior can be expected. See a dynamical systems text, such as Hirsch *et al*. (2012), Izhikevich (2007), or Strogatz (1994) for more information, and for the analogous concept of *Liapunov exponents* for characterizing the stability of limit cycles.

1.12 Perspectives

The subject of computational neuroendocrinology is young, and full of captivating open questions with important medical consequences. To mention just a few: What is the role of the diversity and irregularity of firing patterns observed in secretory neuroendocrine cells? Do they enable interplay between unscheduled perturbations (e.g., stessors in the adrenal corticosteroid system) and endogenous oscillatory rhythms (e.g., on circhoral or circadian scales)? More generally, how are time and space scales crossed from firing patterns to tissue level secretory networks and thence to axis level feedback loops? And how does the beautiful structure of interwoven networks of different cell types in the anterior pituitary contribute to endocrine decision making? It is an exciting area of study, requiring collaboration among neuroscientists, endocrinologists, and mathematical scientists.

This tutorial was designed to help empower that collaboration. Through the lens of the Morris–Lecar model, we have introduced concepts of electrical excitability, mathematical modeling, and dynamical systems. We focused on excitability because neuroscientists have a strong intuition for it, and its graphic spikes and bursts provide an enticing launch pad for mathematical analysis. We worked in two dimensions, because the geometry of the phase plane provides an excellent point of contact for experimentalists and theoreticians, harnessing the visual intuition to help translate between the disciplines.

The modeling and dynamical systems techniques developed are extremely versatile, applying across the neuroendocrine system and in higher dimensions, as shown in the chapters that follow. At the cellular level, Bertram *et al*. model the diverse mechanisms of channel gating found in secretory pituitary cells, and describe the hybrid biological/computational system of the dynamic clamp. Sherman describes how the interaction between membrane potential and calcium dynamics can produce bursting; Sneyd *et al*. present a detailed model of bursting

in GnRH cells and MacGregor and Leng introduce random processes into a dynamical model of firing to understand phasic spiking patterns in vasopressin neurons. Increasing scale to the tissue level, Hodson *et al*. analyze the network structure of cells in the anterior pituitary, and Leng and Feng apply dynamical systems methods to a network of oxytocin cells. Increasing scale again, to the level of whole endocrine axes, Terry *et al*. model feedforward and feedback systems of the stress axis, and Clement and Vidal model the dynamics of GnRH secretion in the female reproductive axis. Increasing scale to the planetary level, the dynamics of excitability are even finding important applications in climate science (Crucifix, 2012).

Acknowledgement

We are grateful to Bowdoin College (Faculty Leave Supplement and Porter Fellowship) and the National Science Foundation (DMS-0940243 and CCF-0832788) for their support of this work.

References

Bean BP (2007). The action potential in mammalian central neurons. *Nat Rev Neurosci.* **8**, 451–465.

Bertram R, Butte MJ, Kiemel T and Sherman A (1995). Topological and phenomenological classification of bursting oscillations. *Bull Math Biol.* **57**, 413–439.

Bertram R, Tabak J, Stojilkovic SS (2014), in press.

Blanchard P, Devaney RL and Hall GR (2011). *Differential Equations.* 4th ed. Brooks/Cole. [*Popular undergraduate text on differential equations and dynamical systems*].

Carrasquillo Y and Nerbonne JM (2014). Diverse regulatory mechanisms. *Neuroscientist* **20**, 104–111.

Coetzee WA, Amarillo Y, Chiu J, Chow A, Lau D, McCormack T, Morena H, Nadal MS, Ozaita A, Pountney D, Saganich M, Vega Saenz de Miera E and Rudy B (1999). Molecular diversity of K^+ channels. *Ann NY Acad Sci.* **868**, 233–285.

Crucifix M (2012). Oscillators and relaxation phenomena in Pleistocene climate theory *Phil Trans R Soc A* **370**, 1140–1165.

Dolphin AC (2009). Calcium channel diversity: multiple roles of calcium channel subunits. *Curr Opin Neurobiol.* **19**, 237–244.

Edelstein-Keshet L (2005). *Mathematical Models in Biology.* Classics in Applied Mathematics, SIAM.

Ellner SP and Guckenheimer J (2006). *Dynamic Models in Biology.* Princeton University Press. Supplementary materials available at http://press.princeton.edu/titles/8124.html.

Ermentrout GB, XPP (2012 or current version) available at http://www.math.pitt.edu/bard/xpp/xpp.html. [*Dynamical systems software package used in the exercises*].

Ermentrout GB and Terman DH (2010). *Mathematical Foundations of Neuroscience.* Springer.

Fall CP, Marland ES, Wagner JM and Tyson JJ (2005). *Computational Cell Biology.* Springer.

Fatt P and Katz B (1953). The electrical properties of crustacean muscle fibres. *J Physiol.* **120**, 171–204.

Fitzhugh R (1961). Impulses and physiological states in theoretical models of nerve membrane. *Biophys J.* **1**, 445–466.

Golubitsky M, Josic K and Kaper TJ (2001). An unfolding theory approach to bursting in fast-slow systems. In *Global Analysis of Dynamical Systems: Festschrift Dedicated to Floris Takens* (eds. Broer HW, Krauskopf B and Vegter G), Chapter 10, pp. 277–308. IOP Publishing Ltd.

González C, Baez-Nieto D, Valencia I, Oyarzún I, Rojas P, Naranjo D and Latorre R (2012). K^+ channels: function-structural overview. *Compr Physiol.* **2**, 2087–2149.

Hille B (2001). *Ion Channels of Excitable Membranes.* 3rd edn. Sinauer Associates, Inc. [*Basic electrophysiology and ion channel biology*].

Hirsch MW, Smale S and Devaney RL (2012). *Differential Equations, Dynamical Systems, and an Introduction to Chaos.* Academic Press.

Hodgkin AL (1948). The local electric changes associated with repetitive action in a non-medullated axon. *J Physiol.* **107**, 165–181.

Hodgkin AL and Huxley AF (1952). A quantitative description of membrane current and its application to conduction and excitation in nerve. *J Physiol.* **117**, 500–544.

Izhikevich EM (2007). *Dynamical Systems in Neuroscience: The Geometry of Excitability and Bursting.* MIT Press, Cambridge, MA. [*Popular introduction to modeling and dynamical systems in neuroscience*].

Jan LY and Jan YN (2012). Voltage-gated potassium channels and the diversity of electrical signalling. *J Physiol.* **590**, 2591–2599.

Jegla TJ, Zmasek CM, Batalov S and Nayak SK (2009). Evolution of the human ion channel set. *Com. Chem. High T. Scr.* **12**, 2–23.

Jones CKRT (1995). Geometric singular perturbation theory, In *Dynamical systems (Montecatini Terme, 1994) Lecture Notes in Mathematics, vol 1609.* (eds. Dold A and Takens G), pp. 44–118. Springer.

Keener J and Sneyd J (2008). *Mathematical Physiology: I: Cellular Physiology.* Springer.

Keynes RD, Rojas E, Taylor RE and Vergara J (1973). Calcium and potassium systems of a giant barnacle muscle fibre under membrane potential control. *J Physiol.* **229**, 409–455.

King JT, Lovell P, Rishniw M, Kotlikoff MI, Zeeman ML and McCobb DP (2006). $\beta 2$ and $\beta 4$ Subunits of BK channels confer differential sensitivity to acute modulation by Steroid hormones. *J Neurophysiol.* **95**, 2878–2888.

Koch C (1999). *Biophysics of Computation: Information Processing in Single Neurons.* Oxford University Press.

Liang Z, Chen L and McClafferty H (2011). Control of hypothalamic-pituitary-adrenal stress axis activity by the intermediate conductance calcium-activated potassium channel, SK4. *J Physiol.* **589**, 5965–5986.

Lipscombe D, Andrade A and Allen SE (2013). Alternative splicing: functional diversity among voltage-gated calcium channels and behavioral consequences. *Biochim Biophys Acta* **1828**, 1522–1529.

Lovell PV, James DG and McCobb DP (2000). Bovine versus rat adrenal chromaffin cells: big differences in BK potassium channel properties. *J Neurophysiol.* **83**, 3277–3286.

Lovell P V, King JT and McCobb DP (2004). Acute modulation of adrenal chromaffin cell BK channel gating and cell excitability by glucocorticoids. *J Neurophysiol.* **91**, 561–570.

Lovell PV and McCobb DP (2001). Pituitary control of BK potassium channel function and intrinsic firing properties of adrenal chromaffin cells. *J Neurosci.* **21**, 3429–3442.

Morris C and Lecar H (1981). Voltage oscillations in the barnacle giant muscle fiber. *Biophys J.* **35**, 193–213. [*Original description of the Morris–Lecar model*].

Nagumo J, Arimoto S, and Yoshizawa S (1962). An active pulse transmission line simulating nerve axon. *Proc IRE* **50**, 2061–2070.

Pongs O and Schwarz JR (2010). Ancillary subunits associated with voltage-dependent K+ channels. *Physiol Rev.* **90**, 755–796.

Rinzel J and Ermentrout GB (1989). Analysis of neural excitability and oscillations. In *Methods in Neuronal Modeling* (eds. Koch C and Segev I), pp. 251–291. MIT Press, Cambridge, MA. [*Seminal paper on bifurcations in the Morris–Lecar model on which this tutorial is based.*]

Sherman A (2011). Dynamical systems theory in physiology. *J Gen Physiol.* **138**, 13–19.

Stojilkovic SS, Tabak J and Bertram R (2010). Ion channels and signaling in the pituitary gland. *Endocr Rev.* **31**, 845–915.

Strogatz SH (1994). *Nonlinear Dynamics and Chaos: With Applications to Physics, Biology, Chemistry, and Engineering*. Perseus Books Publishing, LLC. [*Popular text on dynamical systems with applications across the sciences.*]

Tian L and Shipston MJ (2000). Characterization of hyperpolarization-activated cation currents in mouse anterior pituitary, AtT20 D16:16 corticotropes. *Endocrinology* **141**, 2930–2937.

Vacher H and Trimmer JS (2011). Diverse roles for auxiliary subunits in phosphorylation-dependent regulation of mammalian brain voltage-gated potassium channels. *Pflugers Arch.* **462**, 631–643.

Xu K, Terakawa S (1999). Fenestration nodes and the wide submyelinic space form the basis for the unusually fast impulse conduction of shrimp myelinated axons. *J Exp Biol.* **202**, 1979–1989.

Zakon HH (2012). Adaptive evolution of voltage-gated sodium channels: the first 800 million years. *Proc Natl Acad Sci – USA* **109** Suppl, 10619–10625.

Zeeman EC (1977). *Catastrophe Theory: Selected Papers, 1972–1977.* Addison-Wesley.